COLLEGE PARK CAMPUS

A MODEL STUDY OF ELEMENT RESIDUAL ESTIMATORS FOR LINEAR ELLIPTIC PROBLEMS: THE QUALITY OF THE ESTIMATORS IN THE INTERIOR OF MESHES OF TRIANGLES AND QUADRILATERALS

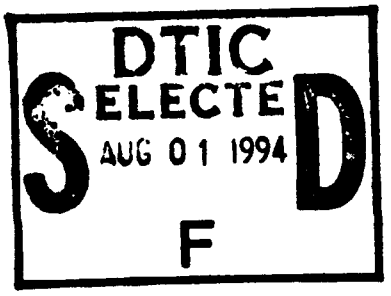

by

I. Babuška
T. Strouboulis
C. S. Upadhyay
S. K. Gangaraj

Technical Note BN-1171

and

CMC Report No. 94-04
Texas Engineering Experiment Station
The Texas A&M University System

May 1994

INSTITUTE FOR PHYSICAL SCIENCE AND TECHNOLOGY

SECURITY CLASSIFICATION OF THIS PAGE (When Data Entered)

REPORT DOCUMENTATION PAGE		READ INSTRUCTIONS BEFORE COMPLETING FORM
1. REPORT NUMBER Technical Note BN-1171	2. GOVT ACCESSION NO.	3. RECIPIENT'S CATALOG NUMBER
4. TITLE (and Subtitle) A Model Study of Element Residual Estimators for Linear Elliptic Problems: The Quality of the Estimators in the Interior of Meshes of Triangles and Quadrilaterals		5. TYPE OF REPORT & PERIOD COVERED Final Life of Contract 6. PERFORMING ORG. REPORT NUMBER
7. AUTHOR(s) I. Babuska[1] - T. Strouboulis[2] - C. S. Upadhyay S. K. Gangaraj		8. CONTRACT OR GRANT NUMBER(s) [1]N00014-90-J-1030 / ONR & CCR-88-20279 / NSF [2]SEE PAGE 1
9. PERFORMING ORGANIZATION NAME AND ADDRESS Institute for Physical Science and Technology University of Maryland College Park, MD 20742-2431		10. PROGRAM ELEMENT, PROJECT, TASK AREA & WORK UNIT NUMBERS
11. CONTROLLING OFFICE NAME AND ADDRESS Department of the Navy Office of Naval Research Arlington, VA 22217		12. REPORT DATE May 1994 13. NUMBER OF PAGES 87 + Figs. 1 - 6b
14. MONITORING AGENCY NAME & ADDRESS(if different from Controlling Office)		15. SECURITY CLASS. (of this report) 15a. DECLASSIFICATION/DOWNGRADING SCHEDULE

16. DISTRIBUTION STATEMENT (of this Report)

Approved for public release: distribution unlimited

17. DISTRIBUTION STATEMENT (of the abstract entered in Block 20, if different from Report)

18. SUPPLEMENTARY NOTES

19. KEY WORDS (Continue on reverse side if necessary and identify by block number)

20. ABSTRACT

In [1] and [2] we presented a model study of a posteriori error estimators in the interior of finite element meshes using a computer-based methodology. In this paper we investigate further the quality of element-residual error estimators. We analyzed several versions of the element-residual estimator and based on this study we propose recipes for robust estimators.

DD FORM 1 JAN 73 1473 EDITION OF 1 NOV 65 IS OBSOLETE

S N 0102-LF-014-6601

SECURITY CLASSIFICATION OF THIS PAGE (When Data Entered)

A model study of element residual estimators for linear elliptic problems: The quality of the estimators in the interior of meshes of triangles and quadrilaterals

I. Babuška*
Institute for Physical Science and Technology and Department of Mathematics,
University of Maryland, College Park, MD 20742, U.S.A.

T. Strouboulis†, C.S. Upadhyay† and S.K. Gangaraj†
Department of Aerospace Engineering, Texas A&M University,
College Station, TX 77843, U.S.A.

May 1994

*The work of this author was supported by the U.S. Office of Naval Research under Contract N00014-90-J-1030 and by the National Science Foundation under Grant CCR-88-20279.

†The work of these authors was supported by the U.S. Army Research Office under Grant DAAL03-G-028, by the National Science Foundation under Grant MSS-9025110 and by the Texas Advanced Research Program under Grant TARP-71071.

Abstract

In [1] and [2] we presented a model study of a posteriori error estimators in the interior of finite element meshes using a computer-based methodology. In this paper we investigate further the quality of element-residual error estimators. We analyzed several versions of the element-residual estimator and based on this study we propose recipes for robust estimators.

1 Introduction

A-posteriori error estimation has become an important aspect in the practical application of the finite element method. As a result much interest has focused on the design of a-posteriori error estimators, their experimental verification and their use in adaptive procedures; see for example [1-65] and the references therein. There are two major classes of error estimators:

1. *Residual estimators*: These estimators employ the solutions of local boundary-value problems posed in an element or a small patch of elements. The data for the local problems are given by the local residuals. For various versions of element residual estimators see [1-26]. It is also possible to construct residual-type estimators by employing the method of hypercircle [27,30] the aim being to construct a global upper estimate of the error. Estimators of this type have been proposed in [30-44].

2. *Estimators based on local averaging*: Estimators belonging to this class employ a smoothened flux-field which is obtained by some local averaging (post-processing). The smoothened flux is then compared with the finite-element flux to construct an estimate of the error. Estimators of this type are given in [45-62]. It can be shown that estimators based on local averaging can also be interpreted as residual estimators (see [63]). For other types of estimators see [64] and [65].

In this paper we will focus on *element residual estimators*. Let T_h be a mesh and let u_h be a finite element solution for Laplace's equation on this mesh. Let τ denote an interior element of T_h and let us define the following *element-residual* boundary-value problem:

$$\left.\begin{aligned} -\Delta \hat{e}_\tau &= \Delta u_h && \text{in} \quad \tau \\ \frac{\partial \hat{e}_\tau}{\partial n} &= \hat{F}_{\partial\tau} - \frac{\partial u_h}{\partial n} && \text{on} \quad \partial\tau \end{aligned}\right\} \tag{1.1}$$

Here $\hat{F}_{\partial\tau}$ is an approximation of $\dfrac{\partial u}{\partial n}$ which is obtained by post-processing the computed finite element flux in the element and its neighbors such that it satisfies

$$\int_{\partial\tau} \Big(\hat{F}_{\partial\tau} - \frac{\partial u_h}{\partial n}\Big) v + \int_\tau (\Delta u_h) v = 0 \qquad \forall\ v \in \mathcal{P}^q(\tau) \tag{1.2}$$

We will call $\hat{F}_{\partial\tau}$ the *q-order equilibrated flux*. Note that $\hat{F}_{\partial\tau}$ will then automatically satisfy the *consistency condition* (which is obtained from (1.2) by letting $q = 0$) and hence the Neumann problem (1.1) has a solution. Further let $\hat{e}_\tau^{(p+k)} \in S^{p+k}(\tau)$

be an approximate solution, with $S^{p+k}(\tau) \subseteq \mathcal{P}^{p+k}(\tau)$ with $k \geq 1$. We define the *element error indicator*

$$\eta_\tau := |||\hat{e}_\tau^{(p+k)}|||_\tau \tag{1.3}$$

By $|||\cdot|||_\tau$ we mean the energy-norm over the element τ; for the particular case of the Laplacian we have $|||v|||_\tau := ||\,|\nabla v|\,||_{L^2(\tau)}$.

Given a mesh we will denote by ω_0^h a simply connected set of elements and we will refer to it as a *mesh-cell*. The mesh-cell is meant as a typical pattern of elements which appears in several places in the mesh. The word *pattern* refers to *the geometry of the mesh in the mesh-cell and a few surrounding mesh-layers*. We will be interested to study the quality of estimators $\mathcal{E}_{\omega_0^h}$ of the error in ω_0^h, where

$$\mathcal{E}_{\omega_0^h} := \sqrt{\sum_{\tau \in \omega_0^h} \eta_\tau^2} \tag{1.4}$$

The quality will be measured by the effectivity index

$$\kappa_{\omega_0^h} := \frac{\mathcal{E}_{\omega_0^h}}{|||e_h|||_{\omega_0^h}} \tag{1.5}$$

Here $e_h := u_{EX} - u_h$ denotes the exact error. The *global effectivity index*, κ_{T_h}, is obtained from (1.5) by letting $\omega_0^h \equiv T_h$.

Let $\mathcal{U}, \mathcal{T}$ be the class of exact solutions, meshes under consideration and let ω_0^h be a mesh-cell with fixed topology (but not size) which appears in all the meshes in $\mathcal{T}$. We will call the estimator $\mathcal{E}_{\omega_0^h} = \mathcal{E}_{\omega_0^h}$ $(\mathcal{U}, \mathcal{T}, C_L^{\omega_0^h}, C_U^{\omega_0^h})$-*proper* if for any solution $u_{EX} \in \mathcal{U}$ we have

$$C_L^{\omega_0^h}(\mathcal{U}, \mathcal{T}) \leq \kappa_{\omega_0^h} \leq C_U^{\omega_0^h}(\mathcal{U}, \mathcal{T}) \tag{1.6}$$

The estimator is called *asymptotically* $(\mathcal{U}, \mathcal{T})$-*exact* in $\omega_0^{h_i}$ if for any $u_{EX} \in \mathcal{U}$ and any sequence of meshes $\{T_{h_i}\}_{i=1}^{\infty}$ from $\mathcal{T}$, such that

$$|||u_{h_i} - u_{EX}|||_\Omega \longrightarrow 0 \qquad \text{as } i \to \infty \tag{1.7a}$$

we have

$$\kappa_{\omega_0^{h_i}} \longrightarrow 1 \tag{1.7b}$$

Here $\{\omega_0^{h_i}\}_{i=1}^{\infty}$ denotes a sequence of mesh-cells of fixed geometry. If $C_L^{\omega_0^h} \geq 1$ then $\mathcal{E}_{\omega_0^h}$ is called an $(\mathcal{U}, \mathcal{T})$-*upper estimator* and if $C_U^{\omega_0^h} \leq 1$ then $\mathcal{E}_{\omega_0^h}$ is called a $(\mathcal{U}, \mathcal{T})$-*lower estimator*.

We will be interested in the values of $C_L^{\omega_0^h}$, $C_U^{\omega_0^h}$ for which (1.6) holds asymptotically in the limit $h \to 0$ (details about the precise meaning of the limit will be given below). We can then quantify the quality of the estimator in a mesh-cell ω_0^h by defining the *robustness index* in ω_0^h for the class of solutions $\mathcal{U}$ (see also [2])

$$\mathcal{R}_{\omega_0^h}(\mathcal{U}) = max\Big(|1 - C_U^{\omega_0^h}| + |1 - C_L^{\omega_0^h}|, |1 - \frac{1}{C_U^{\omega_0^h}}| + |1 - \frac{1}{C_L^{\omega_0^h}}|\Big) \qquad (1.8)$$

We will say that *the estimator is robust in ω_0^h if the robustness index is sufficiently small* (for example less than 0.5).

In this paper we will study the robustness of element-residual estimators for interior mesh-cells (i.e. for mesh-cells which are separated by a few mesh-layers from the boundary). Moreover we will consider the class of solutions $\mathcal{U}$ which occur in practical engineering computations in two-dimensions i.e. the class of solutions which are infinitely smooth except at a finite number of algebraic-type singularities on the boundary or on the material-interfaces. Further, we will assume that the meshes T_h are constructed adaptively and are nearly equilibrated in the energy-norm. Under these assumptions it is possible to compute the values of $C_L^{\omega_0^h}$, $C_U^{\omega_0^h}$ and $\mathcal{R}_{\omega_0^h}$ using the computer-based methodology given in [1] and [2]. For a given mesh-cell ω_0^h the robustness of an element-residual estimator depends on:

(a) The choice of the solution space $S^{(p+k)}(\tau)$ for the local problem. We will demonstrate that *the best robustness is obtained by selecting $S^{(p+k)}(\tau)$ to be a bubble-space of polynomials of degree $(p+1)$.*

(b) The technique for the construction of the equilibrated boundary-flux $\hat{F}_{\partial\tau}$. We show that *the robustness of the estimator depends on the order q of the equilibrated flux. By letting $q = p$ we obtain the best robustness.*

Below we will study the influence of factors (a), (b) on the robustness of element-residual estimators for the model problems of orthotropic heat-conduction and plane-elasticity.

Following this Introduction we will give preliminaries on the model problems and an outline of the methodology for assessing the robustness of estimators for interior mesh-cells. We describe the element residual estimators implemented, we present the model study of the robustness of the estimators for meshes of triangles and quadrilaterals and we give concrete recommendations about which versions of the element residual estimators are robust and should be employed in practical computations.

2 The model problems

We shall consider the vector-valued boundary-value problem

$$\left.\begin{aligned} L_i(\boldsymbol{u}) := -\sum_{j=1}^{2} \frac{\partial}{\partial x_j}\big(\sigma_{ij}(\boldsymbol{u})\big) = f_i \qquad & \text{in } \Omega \\ u_i = 0 \qquad & \text{on } \Gamma_D \\ \sum_{j=1}^{2} \sigma_{ij}(\boldsymbol{u}) n_j = \bar{t}_i \qquad & \text{on } \Gamma_N \end{aligned}\right\} \tag{2.1}$$

where $i = 1, 2$.

Here $\Omega \subset \mathbf{R}^2$ is a bounded domain with boundary $\partial\Omega = \Gamma_D \cup \Gamma_N$;

$\boldsymbol{n} := (n_1, n_2)$ is the outward pointing unit-normal on Γ_N;

f_i, $i = 1, 2$ are the components of the load-vector (*body-force*);

$\bar{t}_i$, $i = 1, 2$ are the components of the normal-flux vector (*traction*) applied on Γ_N;

$\Gamma_D \neq \emptyset$, $\Gamma_D \cap \Gamma_N = \emptyset$; $\boldsymbol{u} = (u_1, u_2)$ is the solution-vector (*displacement*);

$$\epsilon_{ij}(\boldsymbol{u}) := \frac{1}{2}\left(\frac{\partial u_i}{\partial x_j} + \frac{\partial u_j}{\partial x_i}\right), \qquad \sigma_{ij}(\boldsymbol{u}) := \sum_{k,\ell=1}^{2} a_{ijk\ell}\, \epsilon_{k\ell}(\boldsymbol{u}), \qquad i, j = 1, 2 \tag{2.2}$$

are the components of the flux (*strain, stress*);

$a_{ijk\ell}$, $i, j, k, \ell = 1, 2$, are the material-coefficients (*elastic constants*) which in the case of isotropic plane elasticity are given by $a_{ijk\ell} = \mu(\delta_{ij}\delta_{k\ell} + \delta_{i\ell}\delta_{kj}) + \lambda\delta_{ik}\delta_{j\ell}$ where δ_{ij} is Kronecker's delta and λ, μ are Lamé's constants.

We also introduce the scalar elliptic boundary-value problem (*heat-conduction in orthotropic medium*), namely

$$\left.\begin{aligned} \mathcal{L}(u) := -\sum_{k,\ell=1}^{2} \frac{\partial}{\partial x_k}\left(K_{k\ell}\frac{\partial u}{\partial x_\ell}\right) = f \qquad & \text{in } \Omega \\ u = 0 \qquad & \text{on } \Gamma_D \\ \sum_{k=1}^{2} q_k(u) n_k = \bar{g} \qquad & \text{on } \Gamma_N \end{aligned}\right\} \tag{2.3}$$

Here f denotes the *heat-source*; $\bar{g}$ is the *boundary heat-flux*; $q_k(u) := \sum_{\ell=1}^{2} K_{k\ell}\frac{\partial u}{\partial x_\ell}$, $k = 1,2$ are the components of the flux-vector (*heat-flux*) and $K_{k\ell}$, $k,\ell = 1,2$, are the entries of the *thermal-conductivity matrix* which is symmetric, positive definite. We will denote the principal values of the thermal-conductivity matrix by K_{min}, K_{max}.

Let us now cast the model problems in variational form. Let us denote the space of test-functions by

$$\boldsymbol{H}^1_{\Gamma_D} := \left\{ \boldsymbol{v} = (v_1, v_2) \;\middle|\; v_i \in H^1(\Omega),\ v_i = 0 \text{ on } \Gamma_D \right\} \tag{2.4}$$

The variational form of the boundary-value problem (2.1) is now posed as:

Find $\boldsymbol{u} \in \boldsymbol{H}^1_{\Gamma_D}$ such that

$$B_\Omega(\boldsymbol{u}, \boldsymbol{v}) = \int_\Omega \sum_{i=1}^{2} f_i v_i + \int_{\Gamma_N} \sum_{i=1}^{2} \bar{t}_i v_i \qquad \forall\, \boldsymbol{v} \in \boldsymbol{H}^1_{\Gamma_D} \tag{2.5}$$

where the bilinear form $B_\Omega : \boldsymbol{H}^1_{\Gamma_D} \times \boldsymbol{H}^1_{\Gamma_D} \to \boldsymbol{R}$ is defined by

$$B_\Omega(\boldsymbol{u}, \boldsymbol{v}) := \int_\Omega \sum_{i,j,k,\ell=1}^{2} a_{ijk\ell}\frac{\partial u_j}{\partial x_\ell}\frac{\partial v_i}{\partial x_k} \tag{2.6}$$

The energy-norm over any subdomain $S \subseteq \Omega$ is defined by

$$|||\boldsymbol{v}|||_S := \sqrt{B_S(\boldsymbol{v}, \boldsymbol{v})} \tag{2.7}$$

where $B_S(\boldsymbol{u}, \boldsymbol{v})$ has the obvious meaning.

In the case of the scalar elliptic problem given by (2.3) the bilinear form is given by $b_\Omega(u, v) := \int_\Omega \sum_{k,\ell=1}^{2} K_{k\ell}\frac{\partial u}{\partial x_\ell}\frac{\partial v}{\partial x_k}$. The weak-solution of (2.3) satisfies:

Find $u \in H^1_{\Gamma_D} := \left\{ v \in H^1(\Omega) \;\middle|\; v = 0 \text{ on } \Gamma_D \right\}$ such that

$$b_\Omega(u, v) = \int_\Omega fv + \int_{\Gamma_N} \bar{g}v \qquad \forall\, v \in H^1_{\Gamma_D} \tag{2.8}$$

The energy-norm in any subdomain $S \subseteq \Omega$ is defined by $|||v|||_S := \sqrt{b_S(v, v)}$.

Let $\mathcal{T} = \{T_h\}$ be a family of meshes of triangles or quadrilaterals with straight edges. It is assumed that the family is regular. (For the triangles the minimal angle of all the triangles is bounded below by a positive constant, the same for all the meshes. For the quadrilaterals see conditions (37.40) in Ciarlet [67].) Here we will employ only meshes of squares with local refinements; for a description of the

properties of the meshes and the corresponding finite element spaces see [10], [12], [13], [15], [76]. We introduce the conforming finite-element spaces for the scalar model problem:

$$S_h^p(T_h) := \left\{ u \in C^0(\Omega) \,\middle|\, u|_{\tau_k} \in S_h^p(\tau_k), \quad k = 1, \ldots, M(T_h) \right\}, \tag{2.9}$$

The corresponding spaces of vector-valued functions for the elasticity problem are defined similarly. Here $S_h^p(\tau_k)$ denotes the *finite-element space* over τ_k. For the meshes of triangles $S_h^p(\tau_k) = \mathcal{P}_p(\tau_k)$, while for the meshes of quadrilaterals

$$S_h^p(\tau_k) := \left\{ w \in C^\infty(\tau_k) \,\middle|\, w \circ \boldsymbol{F}_{\tau_k} \in \hat{S}^p(\hat{\tau}) \right\} \tag{2.10}$$

where $\hat{\tau} := (-1,1)^2$ is the master-element and $\boldsymbol{F}_{\tau_k}$ is the bilinear mapping of $\hat{\tau}$ onto τ_k; $M(T_h)$ is the number of elements in T_h and $\hat{S}^p(\hat{\tau})$ denotes the polynomial space in the master-element.

For the quadrilaterals we will consider the following choices for the definition of the polynomial space $\hat{S}^p(\hat{\tau})$ (see also [76]).

a. Tensor-product (bi-p) polynomial space of degree p.

$$\hat{\mathcal{S}}_{bi-p}^{(p,p)}(\hat{\tau}) := \left\{ \hat{P} \,\middle|\, \hat{P}(\hat{x}_1, \hat{x}_2) = \sum_{\substack{i,j \\ 0 \le i,j \le p}} \alpha_{i,j}\, \hat{x}_1^i\, \hat{x}_2^j \right\} \tag{2.11}$$

b. Serendipity (trunc) polynomial space of degree p.

$$\hat{\mathcal{S}}_{trunc}^{(p,p)}(\hat{\tau}) := \left\{ \hat{P} \,\middle|\, \hat{P}(\hat{x}_1, \hat{x}_2) = \sum_{\substack{i,j \\ 0 \le i+j \le p}} \alpha_{i,j}\, \hat{x}_1^i\, \hat{x}_2^j + \alpha_{p,1}\, \hat{x}_1^p\, \hat{x}_2 + \alpha_{1,p}\, \hat{x}_1\, \hat{x}_2^p \right\} \tag{2.12}$$

c. Intermediate polynomial space of degree p.

$$\hat{\mathcal{S}}_{inter}^{(p,p)}(\hat{\tau}) := \left\{ \hat{P} \,\middle|\, \hat{P}(\hat{x}_1, \hat{x}_2) = \sum_{\substack{i,j \\ 0 \le i+j \le p}} \alpha_{i,j}\, \hat{x}_1^i\, \hat{x}_2^j + \sum_{k=0}^{p-1} \alpha_{p-k,\,k+1}\, \hat{x}_1^{p-k}\, \hat{x}_2^{k+1} \right\} \tag{2.13}$$

We let $S_{h,\Gamma_D}^p := S_h^p(T_h) \cap H_{\Gamma_D}^1$ denote the discrete test-space. The finite element solution u_h (for the heat-conduction problem) satisfies:

Find $u_h \in S_{h,\Gamma_D}^p$ such that

$$b_\Omega(u_h, v_h) = \int_\Omega f v_h + \int_{\Gamma_N} \bar{g} v_h \qquad \forall\, v_h \in S_{h,\Gamma_D}^p \tag{2.14}$$

The error is $e_h := u - u_h$. The finite element solution and the error for the elasticity problem are defined similarly.

The error satisfies the *residual-equation*:

$$b_\Omega(e_h, v_h) = \sum_{\tau \in T_h} \mathcal{F}_\tau(v_h) \qquad \forall\ v_h \in H^1_{\Gamma_D} \tag{2.15}$$

where the residual-functional for element τ is defined by

$$\mathcal{F}_\tau(v) := \int_\tau r_\tau v + \sum_{\epsilon \in E(\tau)} \int_\epsilon \frac{1}{2} J_\epsilon v\,, \quad v \in H^1(\tau) \tag{2.16}$$

where $E(\tau)$ is the set of edges for element τ, r_τ is the *interior-residual* in element τ,

$$r_\tau := -\mathcal{L}(u_h|_\tau) + f \tag{2.17}$$

and J_ϵ is the *jump* or *edge-residual* associated with the edge ϵ

$$J_\epsilon := \begin{cases} [q(u_h|_{\tau_{in}}) - q(u_h|_{\tau_{out}})] \cdot \boldsymbol{n}\,, & \epsilon \in E_{int} \\ \\ 2[\bar{g} - q(u_h|_{\tau_{out}}) \cdot \boldsymbol{n}]\,, & \epsilon \subseteq \Gamma_N \end{cases} \tag{2.18}$$

Here E_{int} denote the set of edges in the interior of the domain $\boldsymbol{n}$ denotes the unit-normal assigned to the edge ϵ and τ_{in}, τ_{out} denote the elements attached to the edge, as shown in Fig. 1.

3 Outline of the theoretical setting

The theoretical setting will be outlined below (for the details see [1]) for the special class of *locally periodic meshes* which are defined as follows. Let $0 < H < H^0$, $\boldsymbol{x}^0 = (x_1^0, x_2^0) \in \Omega$,

$$S(\boldsymbol{x}^0, H) := \left\{ \boldsymbol{x} = (x_1, x_2) \middle|\ |x_i - x_i^0| < H\,, \quad i = 1,2 \right\} \tag{3.1}$$

and assume H^0 is sufficiently small such that $\bar{S}(\boldsymbol{x}^0, H^0) \subset \Omega$. Further, let γ be a set of multi-indices (i,j), $\boldsymbol{x}^{(i,j)} = (x_1^{(i,j)}, x_2^{(i,j)}) \in \Omega$ and

$$c(\boldsymbol{x}^{(i,j)}, h) := S(\boldsymbol{x}^{(i,j)}, h) \subset S(\boldsymbol{x}^0, H)\,, \qquad (i,j) \in \gamma \tag{3.2}$$

be the set of the h-cells (or cells) which cover exactly $S(\boldsymbol{x}^0, H)$, as is for example shown in Fig. 2. We will refer to $S(\boldsymbol{x}^0, H)$ as *the subdomain of periodicity of the mesh centered at* $\boldsymbol{x}^0$. We will denote by $\tilde{c} := S(\mathbf{0}, 1)$ the *unit-* (*master-*) cell $\tilde{c}$, the h-cell is an h-scaled and translated master-cell.

Let $\tilde{T}$ be a mesh of triangles or squares on the master-cell (the master-mesh) and $\tilde{T}_h^{(i,j)}$ be the mesh on $c(\boldsymbol{x}^{(i,j)}, h)$ which is the scaled and translated image of $\tilde{T}$. We will consider the family $\mathcal{T}$ of locally periodic meshes. Let $T_h \in \mathcal{T}$ and $T_h(\boldsymbol{x}^0, H)$ be the restriction of T_h on $S(\boldsymbol{x}, H)$ and $T_h^{(i,j)}$ the restriction of $T_h(\boldsymbol{x}^0, H)$ on $c(\boldsymbol{x}^{(i,j)}, h)$. We assume that $T_h^{(i,j)} = \tilde{T}_h^{(i,j)}$, $(i,j) \in \gamma$ i.e. $T_h(\boldsymbol{x}^0, H)$ is made by the periodic repetition of the h-scaled master mesh. Outside the subdomain $S(\boldsymbol{x}^0, H)$ the mesh is arbitrary; it could have curved elements, refinements, etc.

Let Q be a polynomial of degree $(p+1)$ defined over the master-cell $\tilde{c}$ and let $\tilde{T}$ be the master-mesh. Then denote

$$\rho := Q - Q_1^{\mathrm{INT}} \tag{3.3}$$

where Q_1^{INT} is the interpolant of degree p of the function Q defined over the master-mesh $\tilde{T}$ (for which $h = 1$). Any polynomial of degree p on an element τ_k belongs to $S_1^p(\tau_k)$ and hence any polynomial of degree p on $S(\boldsymbol{x}^0, H)$ belongs to $S_1^p(T_h(\boldsymbol{x}^0, H))$. It follows that ρ defined in (3.3) is $\tilde{c}$-periodic (this can be shown exactly as in [1]) and

$$\rho(1, \tilde{x}_2) = \rho(-1, \tilde{x}_2), \qquad |\tilde{x}_2| < 1 \tag{3.4a}$$

$$\rho(\tilde{x}_1, 1) = \rho(\tilde{x}_1, -1), \qquad |\tilde{x}_1| < 1 \tag{3.4b}$$

Let

$$H^1_{\mathrm{PER}}(\tilde{c}) := \left\{ u \in H^1(\tilde{c}) \;\middle|\; u \text{ satisfies (3.4)} \right\} \tag{3.5}$$

and

$$S^p_{1,\mathrm{PER}}(\tilde{c}) := \left\{ u \in H^1_{\mathrm{PER}}(\tilde{c}) \;\middle|\; u|_{\tilde{\tau}} \in S_1^p(\tilde{\tau}), \quad \forall\ \tilde{\tau} \in \tilde{T} \right\} \tag{3.6}$$

Further let $\tilde{z}^\rho \in S^1_{\mathrm{PER}}(\tilde{c})$ such that

$$b_{\tilde{c}}(\tilde{z}^\rho, \tilde{v}) = b_{\tilde{c}}(\rho, \tilde{v}) \qquad \forall\ \tilde{v} \in S^p_{1,\mathrm{PER}}(\tilde{c}) \tag{3.7a}$$

and

$$\int_{\tilde{c}} (\rho - \tilde{z}^\rho) = 0 \tag{3.7b}$$

Note that the function $\tilde{z}^\rho$ exists and is uniquely determined (we will compute it numerically in the examples). Let us also define $\psi \in H^1(\tilde{c})$ by

$$\psi := \rho - \tilde{z}^\rho = Q - \tilde{w} \quad \text{where} \quad \tilde{w} := Q_1^{\mathrm{INT}} + \tilde{z}^\rho \tag{3.8}$$

Let $\psi_h \in H^1_{\mathrm{PER}}(c(\boldsymbol{x}^{(i,j)}, h))$ be the function ψ, defined above, scaled and translated onto the cell $c(\boldsymbol{x}^{(i,j)}, h)$ of the mesh in $S(\boldsymbol{x}^0, H)$ i.e.

$$\psi_h(\boldsymbol{x}) := h^{p+1}\,\psi(\tilde{\boldsymbol{x}}), \qquad \frac{\partial \psi_h}{\partial x_i}(\boldsymbol{x}) = h^p \frac{\partial \psi}{\partial \tilde{x}_i}(\tilde{\boldsymbol{x}}), \quad i = 1,2, \tag{3.9}$$

where $\tilde{\boldsymbol{x}} = \dfrac{1}{h}(\boldsymbol{x} - \boldsymbol{x}^{(i,j)})$, $\boldsymbol{x} \in c(\boldsymbol{x}^{(i,j)}, h)$. It is easy to see that ψ_h can be periodically extended over $S(\boldsymbol{x}^0, H_1)$. We will also let $w_h(\boldsymbol{x}) := \tilde{w}(\tilde{\boldsymbol{x}})$.

In [75] we proved the following theorem for Poisson's equation based on *the theory of interior estimates* (see [69]):

Theorem 1. Let $H_1 < H < H^0$ and assume that the following assumptions hold with

$$\alpha = \frac{6p+1}{6p}, \qquad \beta = p+1-\epsilon, \qquad \epsilon = \sigma_0 = \frac{1}{6(6p+1)} \tag{3.10}$$

Assume that the exact solution u satisfies

$$\|D^\alpha u\|_{L^\infty(S(x^0,H))} \le K < \infty, \qquad 0 \le |\alpha| \le p+2 \tag{3.11a}$$

where $\alpha := (\alpha_1, \alpha_2)$, $D^\alpha u := \dfrac{\partial^{|\alpha|} u}{\partial x_1^{\alpha_1}\, \partial x_2^{\alpha_2}}$, $|\alpha| := \alpha_1 + \alpha_2$, and

$$R^2 = \sum_{|\alpha|=p+1} a_\alpha^2 > 0 \qquad \text{where} \qquad a_\alpha := (D^\alpha u)(x^0) \tag{3.11b}$$

Further assume that the mesh T_h is such that

$$\|e_h\|_{L^2(S(x^0,H_1))} \le C h^\beta H_1, \qquad \text{with} \quad \beta \ge (p+1) - \epsilon \tag{3.12}$$

Moreover assume that the meshes T_h in $S(\boldsymbol{x}^0, H)$ are such that

$$C_1 H_1^\alpha \le h \le C_2 H_1^\alpha \tag{3.13}$$

Then for any $\boldsymbol{x} \in S(\boldsymbol{x}^0, H_1)$

$$\left|\frac{\partial e_h}{\partial x_i}(\boldsymbol{x})\right| = \left|\frac{\partial \psi_h}{\partial x_i}(\boldsymbol{x})\right| + \lambda C h^{p+\sigma_0} \tag{3.14}$$

with $\sigma_0 > 0$, $|\lambda| \le 1$ and C independent of h.

Theorem 2. Let the assumptions of Theorem 1 hold. Then

$$|||u_h - w_h|||_{S(x^0,H_1)} = |||u_h - Q_h^{INT} - \tilde{z}_h^\rho|||_{S(x^0,H_1)} \le C h^{\sigma_1} |||\psi|||_{S(x^0,H_1)} \tag{3.15}$$

where C is independent of H and h and $\sigma_1 > 0$. See [1] for details of the proof.

Remark 3.1. The theorems assume that the mesh is periodic and that the solution is smooth in a small subdomain (i.e. $S(\boldsymbol{x}^0, H)$) in the interior of the domain. Outside the subdomain we assume neither periodicity of the mesh nor smoothness of the solution. The solution may have algebraic-type singularities at a finite number of corner points or points of abrupt change in the type of boundary-condition. Here it is only assumed that the pollution-error in a shrinking mesh-patch (i.e. $T_h(\boldsymbol{x}^0, H_1)$) in the interior of the subdomain is controlled; this implies that the mesh has been adequately refined in the neighborhood of all singular points. *If the mesh is constructed adaptively to be nearly equilibrated in the energy norm it will satisfy this assumption, for all practical purposes.*

Theorem 3. Assume that the assumptions of Theorem 1 hold. Further assume that for the estimators,

$$\kappa(c(\boldsymbol{x}^0, h), w_h, \mathcal{L}Q) = \frac{\mathcal{E}_{c(\boldsymbol{x}^0,h)}(w_h, \mathcal{L}Q)}{|||\psi|||_{c(\boldsymbol{x}^0,h)}} \geq \alpha > 0 \tag{3.18a}$$

Then

$$\kappa^2(S(\boldsymbol{x}^0, H_1), u_h, f) = \kappa^2(c(\boldsymbol{x}^0, h), w_h, \mathcal{L}Q)(1 + C\lambda h^{\sigma_1}) \tag{3.18b}$$

and

$$\kappa(c(\boldsymbol{x}^0, h), w_h, \mathcal{L}Q) = \kappa(\tilde{c}, \tilde{w}, \mathcal{L}Q) \tag{3.18c}$$

where $\kappa^2(S(\boldsymbol{x}^0, H_2), u_h, f) := (\kappa(S(\boldsymbol{x}^0, H_2), u_h, f))^2$.

Remark 3.2. The proof of theorem 1 in [1] is based on various interior estimates for the error in finite element approximations of Poisson's equation, especially the results given in [69]. It is very plausible that analogs of these results hold for finite element approximations of the elasticity equations and more general elliptic-systems because the main ideas of the proofs of these results carry to the general case. To our knowledge the precise details for the elasticity equations are not available in the open literature. Nevertheless we will assume the validity of the analog of Theorems 1-3 for the equations of elasticity.

4 Description of the element-residual error estimators

Below, we will describe various versions of the element-residual estimator which were tested in this model study. We define the estimators for the scalar model problem; the corresponding definitions of the estimators for the elasticity problem can be constructed analogously.

4.1 Unequilibrated element-residual with $(p+1)$-degree bubble-space

For an interior element τ we consider the following discrete local problem:

Find $\tilde{e}_\tau^{(p+1)} \in M_p^{p+1}(\tau)$ such that

$$b_\tau(\tilde{e}_\tau^{(p+1)}, v) = \mathcal{F}_\tau(v) \qquad \forall\ v \in M_p^{p+1}(\tau) \tag{4.1}$$

Here $M_p^{p+1}(\tau)$ is the *bubble-space* of degree $(p+1)$,

$$M_p^{p+1}(\tau) := \left\{ v \in \mathcal{P}^{p+1}(\tau) \;\middle|\; \Pi_\tau^p(v) = 0 \right\} \tag{4.2}$$

where Π_τ^p is the *element interpolation-operator* defined in [14]. The bubble space can be written as the following algebraic sum:

$$M_p^{p+1}(\tau) = (M_p^{p+1})^b(\tau) \oplus \mathcal{P}_0^{p+1}(\tau) \tag{4.3}$$

Here $\mathcal{P}_0^{p+1}(\tau) := \mathcal{P}^{p+1}(\tau) \bigcap H_0^1(\tau)$ and

$$(M_p^{p+1})^b(\tau) := \left\{ v \in \mathcal{P}^{p+1}(\tau) \;\middle|\; v = \sum_{i=1}^{3} \alpha_i \psi_{\epsilon_i^\tau} \right\} \tag{4.4a}$$

where ϵ_i^τ is the i-th edge of the element τ and $\psi_{\epsilon_i^\tau} \in \mathcal{P}^{p+1}(\tau)$ such that

$$\int_{\epsilon_i^\tau} \frac{\partial \psi_{\epsilon_i^\tau}}{\partial s} \frac{\partial w}{\partial s} = 0 \qquad \forall\ w \in \mathcal{P}_0^p(\epsilon_i^\tau) := \mathcal{P}^p(\epsilon_i^\tau) \bigcap H_0^1(\epsilon_i^\tau) \tag{4.4b}$$

The element error indicators for the unequilibrated element-residual are given by

$$\tilde{\eta}_\tau^{(p+1)} := |||\tilde{e}_\tau^{(p+1)}|||_\tau \tag{4.5}$$

4.2 Construction of the equilibrated residuals

Let us assume that the element-residuals have been modified in the following way:

$$\mathcal{F}_\tau^{EQ}(v) := \mathcal{F}_\tau(v) + \sum_{\epsilon \subseteq \partial\tau \cap E_{int}} \int_\epsilon v \theta_\tau^\epsilon \tag{4.6}$$

Here θ_τ^ϵ is the *correction* for the edge ϵ and the element τ. For any interior edge $\epsilon = \partial\tau \bigcap \partial\tau^*$ it is assumed that $\theta_\tau^\epsilon = -\theta_{\tau^*}^\epsilon$. We then have

$$\sum_{\tau \in T_h} \mathcal{F}_\tau(v) = \sum_{\tau \in T_h} \mathcal{F}_\tau^{EQ}(v) \tag{4.7}$$

In particular if the corrections are such that

$$\mathcal{F}_\tau^{EQ}(1) = 0 \quad \forall\ \tau \in T_h \tag{4.8}$$

we can construct the element-residual problems:

Find $\hat{e}_\tau \in H^1(\tau)$ such that

$$b_\tau(\hat{e}_\tau, v) = \mathcal{F}_\tau^{EQ}(v) \quad \forall\ v \in H^1(\tau) \tag{4.9}$$

We then have

$$|||e_h|||_\Omega = \sup_{v \in H^1_{\Gamma_D}} \frac{\sum_{\tau \in T_h} b_\tau(e_h, v)}{|||v|||_\Omega} = \sup_{v \in H^1_{\Gamma_D}} \frac{\sum_{\tau \in T_h} \mathcal{F}_\tau(v)}{|||v|||_\Omega} = \sup_{v \in H^1_{\Gamma_D}} \frac{\sum_{\tau \in T_h} \mathcal{F}_\tau^{EQ}(v)}{|||v|||_\Omega} \tag{4.10a}$$

and hence

$$|||e_h|||_\Omega = \sup_{v \in H^1_{\Gamma_D}} \frac{\sum_{\tau \in T_h} b_\tau(\hat{e}_\tau, v)}{|||v|||} \leq \sqrt{\sum_{\tau \in T_h} |||\hat{e}_\tau|||_\tau^2} \tag{4.10b}$$

Thus a *global upper-estimator is obtained provided that the local problems are solved exactly*. This motivated various authors [31-44] to construct equilibrated residuals.

We will now outline a recipe for the local construction of equilibrated element-residuals; this technique was proposed in [31-33] (see also [38]-[41]). Following [11] let θ^ϵ be a function defined on each edge ϵ. We define (see Fig. 1)

$$\theta^\epsilon_{\tau_{out}} = \theta^\epsilon\ , \quad \theta^\epsilon_{\tau_{out}} = -\theta^\epsilon \tag{4.11}$$

Given any interior element τ and q, $0 \leq q \leq p$, the aim is to determine edgewise smooth functions θ^ϵ, $\epsilon \in E_{int}$ such that

$$\mathcal{F}_\tau^{EQ}(v) = 0 \qquad \forall\ v \in \mathcal{P}^q(\tau) \tag{4.12}$$

The residual which satisfy (4.12) are said to be *q-order equilibrated*. Eq. (4.12) will hold if

$$\sum_{\epsilon \subseteq \partial\tau} \int_\epsilon \theta^\epsilon_\tau \phi_i = -\mathcal{F}_\tau(\phi_i)\ , \qquad i = 1, \ldots, N^q_\tau \tag{4.13}$$

where ϕ_i is the i-th shape-function of the element and N_τ^q denotes the total number of hierarchic shape-functions of degree q in the element τ. A set of edgewise polynomial corrections for edges in the interior of the mesh is constructed as follows:

(a). Edgewise linear corrections.

Let us first determine edgewise linear corrections in the form

$$\theta^\epsilon = (\theta^{\epsilon,1}\psi_1^\epsilon + \theta^{\epsilon,2}\psi_2^\epsilon) \tag{4.14}$$

$$\psi_1^\epsilon := \frac{2}{|\epsilon|}(2\lambda_1^\epsilon - \lambda_2^\epsilon), \qquad \psi_2^\epsilon := \frac{2}{|\epsilon|}(2\lambda_2^\epsilon - \lambda_1^\epsilon) \tag{4.15}$$

where λ_k^ϵ, $k = 1, 2$ are the linear shape-functions defined over the edge ϵ. Note that

$$\theta^{\epsilon,k} = \int_\epsilon \theta^\epsilon \lambda_k^\epsilon \,, \qquad k = 1,2 \tag{4.16}$$

Let X denote an interior vertex of the mesh with the element τ_i^X and the edges ϵ_i^X, $i = 1, \ldots, 4$, connected to it, as shown in Fig. 3 and let $\nu(\epsilon_k^X)$ denote the local number (1 or 2) of the vertex X with respect to the edge ϵ_k^X. The values of $\theta^{\epsilon_k^X, \nu(\epsilon_k^X)}$ are obtained from the linear system

$$\sum_{\epsilon \subseteq \partial \tau_k^X} \int_\epsilon \theta_{\tau_k^X}^\epsilon \phi_X = -\mathcal{F}_{\tau_k^X}(\phi_X) \,, \qquad k = 1, \ldots, 4 \tag{4.17}$$

which reads

$$\begin{bmatrix} 1 & 0 & 0 & -1 \\ -1 & 1 & 0 & 0 \\ 0 & -1 & 1 & 0 \\ 0 & 0 & -1 & 1 \end{bmatrix} \begin{Bmatrix} \theta^{\epsilon_1^X, \nu(\epsilon_1^X)} \\ \theta^{\epsilon_2^X, \nu(\epsilon_2^X)} \\ \theta^{\epsilon_3^X, \nu(\epsilon_3^X)} \\ \theta^{\epsilon_4^X, \nu(\epsilon_4^X)} \end{Bmatrix} = \begin{Bmatrix} -\mathcal{F}_{\tau_1^X}(\phi_X) \\ -\mathcal{F}_{\tau_2^X}(\phi_X) \\ -\mathcal{F}_{\tau_3^X}(\phi_X) \\ -\mathcal{F}_{\tau_4^X}(\phi_X) \end{Bmatrix} \tag{4.18}$$

Here we assumed that the directions of edge-normals are the ones shown in Fig. 3.

The matrix has exactly one zero eigenvalue with corresponding eigenvector $[1, 1, 1, 1]^T$. Moreover from the ***orthogonality condition*** we have

$$\sum_{k=1}^{4} \mathcal{F}_\tau(\phi_X) = 0 \tag{4.19}$$

and the system is consistent. Particular solutions can be obtained by different choices of the free-constant. For example one may choose $\theta^{\epsilon_4^X, \nu(\epsilon_4^X)} = 0$ (e.g. [11])

or one may choose the constant by minimizing various norms of the solution of (4.18), namely

$$J(\{\theta^{\epsilon_k^X,\nu(\epsilon_k^X)}\}_{k=1}^4) = \sum_{k=1}^4 w_k(\theta^{\epsilon_k^X,\nu(\epsilon_k^X)})^2 \tag{4.20}$$

In [33] it was suggested to let $w_k = 1$ while the choice $w_k = \frac{1}{|\epsilon_k^X|}$ was proposed in [38-39].

b. Higher-order corrections.

Let us denote by $\phi_{\epsilon,k}$, $k = 1,\ldots,(q+1)$ the basis-functions which do not vanish on the edge ϵ. We extend the conjugate basis introduced in (4.15) as follows:

$$\int_\epsilon \psi_i^\epsilon \phi_{\epsilon,j} = \begin{cases} 0, & \text{if } j < i \\ \\ 1, & \text{if } j = 1 \end{cases} \tag{4.21}$$

where $3 \leq i,j \leq (q+1)$.

After the linear edge corrections have been determined, the higher-order corrections can be computed from

$$\theta^{\epsilon,i} = -\mathcal{F}_{\tau_{out}}(\phi_{\epsilon,i}) - \sum_{j=1}^{i-1} \theta^{\epsilon,j} \int_\epsilon \psi_j \phi_{\epsilon,i}\,, \quad i = 3,\ldots,(q+1), \quad \epsilon \subseteq \partial\tau_{out} \tag{4.22}$$

Note that the higher-order corrections can be determined explicitly and are defined uniquely for each edge.

4.3 Equilibrated element residual estimators

We will consider the following equilibrated element residual estimators:

a. Element-residual with q-order equilibration and (p+1)-degree bubble-space:

Find $\tilde{e}_\tau^{(p+1),q} \in M_p^{p+1}(\tau)$ such that

$$b_\tau(\tilde{e}_\tau^{(p+1),q}, v) = \mathcal{F}_\tau^{EQ,q}(v) \qquad \forall\ v \in \mathcal{M}_p^{p+1}(\tau) \tag{4.23}$$

where $\mathcal{F}_\tau^{EQ,q}$ denotes the q-order equilibrated residual in the element τ. The corresponding element error-indicators are

$$\tilde{\eta}_\tau^{(p+1),q} := |||\tilde{e}_\tau^{(p+1),q}|||_\tau \tag{4.24}$$

b. Element-residual with q-order equilibration and (p+k)-polynomial space:

Find $\hat{e}_\tau^{(p+k),q} \in \mathcal{P}^{p+k}(\tau)$ such that

$$b_\tau(\hat{e}_\tau^{(p+k),q}, v) = \mathcal{F}_\tau^{EQ,q}(v) \qquad \forall\ v \in \mathcal{P}^{p+k}(\tau) \tag{4.25}$$

with the corresponding element error indicators

$$\hat{\eta}_\tau^{(p+k),q} := |||\hat{e}_\tau^{(p+k),q}|||_\tau \tag{4.26}$$

Remark 4.1: By letting $k \to \infty$ we recover the exact solution $\hat{e}_\tau^q$ of the local problem (4.9) with q-order equilibrated residuals. In most cases, by letting $k = 3$ we obtain element error indicators which are practically the same as the indicators corresponding to the exact solutions of the local problems.

4.4 Determination of the optimal equilibrations

In the Section 4.2 we gave a recipe for the construction of q-order equilibrated residuals which depend upon the choice of a free-constant for each vertex of the mesh. Here we address the question of the selection of the optimal constants for the estimator based on the exact solution of the equilibrated element-residual problem (4.9). This is an upper estimator, as shown in (4.10). ***By optimal constants for this estimator we mean the ones which minimize the upper-bound for the error in*** (4.10b). In the numerical examples we determined the optimal constants in the interior of locally-periodic meshes. We now give an example of how these constants are determined.

Let us consider a periodic-mesh which is constructed by the periodic repetition of the Criss-Cross pattern shown in Fig. 4d. In this pattern we distinguish two types of vertices, namely, vertex X_1 (which is connected to four elements) and vertex X_2 (which is connected to eight elements). Let C_{X_1}, C_{X_2} denote the free-constants associated with the linear edge-corrections (e.g. eq. (4.18)) for vertex X_1, X_2, respectively. The edge-corrections for this mesh-pattern can be written as

$$\theta^e(C_{X_1}, C_{X_2}) = \theta^e(0,0) + C_{X_1}(\theta^e(1,0) - \theta^e(0,0)) + C_{X_2}(\theta^e(0,1) - \theta^e(0,0)) \tag{4.27}$$

Here we let $\theta^e = \theta^e(C_{X_1}, C_{X_2})$ to denote the dependence of the edge-corrections on the free-constants. By superposition we also have

$$\hat{e}_\tau(C_{X_1}, C_{X_2}) = \hat{e}_\tau(0,0) + C_{X_1}(\hat{e}_\tau(1,0) - \hat{e}_\tau(0,0)) + C_{X_2}(\hat{e}_\tau(0,1) - \hat{e}_\tau(0,0)) \tag{4.28}$$

The error estimator in the periodic mesh-cell ω_0^h is given by

$$\mathcal{E}_{\omega_0^h} = \sqrt{\sum_{i=1}^{4} |||\hat{e}_{\tau_i}(C_{X_1}, C_{X_2})|||_{\tau_i}^2} \tag{4.29}$$

The values of the constants which minimize $\mathcal{E}_{\omega_0^h}$ are obtained by solving the system:

$$\begin{bmatrix} K_{X_1X_1} & K_{X_1X_2} \\ K_{X_1X_2} & K_{X_2X_2} \end{bmatrix} \begin{Bmatrix} C_{X_1} \\ C_{X_2} \end{Bmatrix} = \begin{Bmatrix} F_{X_1} \\ F_{X_2} \end{Bmatrix} \tag{4.30a}$$

where

$$\left.\begin{aligned} K_{X_1X_1} &= \sum_{i=1}^{4} b_{\tau_i}(\hat{e}_{\tau_i}(1,0) - \hat{e}_{\tau_i}(0,0), \hat{e}_{\tau_i}(1,0) - \hat{e}_{\tau_i}(0,0)) \\ K_{X_1X_2} &= \sum_{i=1}^{4} b_{\tau_i}(\hat{e}_{\tau_i}(1,0) - \hat{e}_{\tau_i}(0,0), \hat{e}_{\tau_i}(0,1) - \hat{e}_{\tau_i}(0,0)) \\ K_{X_2X_2} &= \sum_{i=1}^{4} b_{\tau_i}(\hat{e}_{\tau_i}(0,1) - \hat{e}_{\tau_i}(0,0), \hat{e}_{\tau_i}(0,1) - \hat{e}_{\tau_i}(0,0)) \\ F_{X_1} &= -\sum_{i=1}^{4} b_{\tau_i}(\hat{e}_{\tau_i}(1,0) - \hat{e}_{\tau_i}(0,0), \hat{e}_{\tau_i}(0,0)) \\ F_{X_2} &= -\sum_{i=1}^{4} b_{\tau_i}(\hat{e}_{\tau_i}(0,1) - \hat{e}_{\tau_i}(0,0), \hat{e}_{\tau_i}(0,0)) \end{aligned}\right\} \tag{4.30b}$$

By employing these constants we get the optimal estimator based on exact solutions of the equilibrated element residual problems.

4.5 Another method of constructing the equilibrated residuals

In [20], [24] and [44] a method for constructing 0-th order equilibrated residuals was given. This method, ***which obtains the equilibrated residuals by splitting the jumps linearly on each edge***, is outlined below for edges in the interior of the mesh:

The aim is to find functions $\mu_\epsilon \in \mathcal{P}^1(\epsilon)$, $\epsilon \in E_{int}$ such that for every τ in the interior of the mesh T_h

$$\begin{aligned} b_\tau(u_h, 1) = \int_\tau f + \sum_{\epsilon \subseteq \partial\tau} \int_\epsilon \frac{1}{2}(g(u_h|_\tau) + g(u_h|_{\tau^*})) \cdot n_\tau \\ + \sum_{\epsilon \subseteq \partial\tau} \int_\epsilon \mu_\tau^\epsilon J_\epsilon \end{aligned} \tag{4.31}$$

Here μ_τ^ϵ is defined by using the convention $\mu_{\tau_{out}}^\epsilon = -\mu_{\tau_{in}}^\epsilon = \mu^\epsilon$.

We let

$$\mu^\epsilon = \mu^{\epsilon,1}\lambda_1^\epsilon + \mu^{\epsilon,2}\lambda_2^\epsilon \tag{4.32}$$

Then eq. (4.31) can be written as

$$\sum_{\epsilon \subseteq \partial\tau \bigcap E_{int}} \left(\sum_{i=1}^{2} \int_\epsilon \mu^{\epsilon,i}\lambda_i^\epsilon J_\epsilon \right) = -\mathcal{F}_\tau(1) \tag{4.33}$$

Eq. (4.33) will be satisfied if for each vertex X we obtain the values of $\mu^{\epsilon_k^X,\nu(\epsilon_k^X)}$ by solving the linear system:

$$\mu^{\epsilon_k^X,\nu(\epsilon_k^X)} \int_{\epsilon_k^X} \phi_X J_{\epsilon_k^X} - \mu^{\epsilon_{k-1}^X,\nu(\epsilon_{k-1}^X)} \int_{\epsilon_{k-1}^X} \phi_X J_{\epsilon_{k-1}^X} = -\mathcal{F}\tau_k^X(\phi_X), \quad k = 1,\ldots,N_X \tag{4.35}$$

Here we employ the same notation as in Section 4.2. N_X denotes the number of elements connected to vertex X and we define $\epsilon_0^X := \epsilon_{N_X}^X$. By letting

$$\hat{\mu}^{\epsilon_k^X,\nu(\epsilon_k^X)} := \mu^{\epsilon_k^X,\nu(\epsilon_k^X)} \int_{\epsilon_k^X} \phi_X J_{\epsilon_k^X} \tag{4.36}$$

we see that the $\hat{\mu}$-unknowns satisfy the same linear system as the θ-unknowns in Section 4.18. For the details related to the computation of the μ-unknowns see [44].

The 0th-order equilibrated residuals are given by

$$\mathcal{F}_\tau^{EQ,0}(v) := \mathcal{F}_\tau(v) + \sum_{\epsilon \subseteq \partial\tau \bigcap E_{int}} \int_\epsilon \mu_\tau^\epsilon J_\epsilon \tag{4.37}$$

5 Assessment of the quality of the element residual estimator

In this Section we analyze the quality of the element residual estimators, given in the previous Section, for the periodic mesh-patterns shown in Figs. 4a-d. According to Theorem 3, we can compute the asymptotic value of the effectivity index for a mesh-cell in the interior of a periodic mesh-patch from the master-cell, namely

$$\lim_{h \to 0} \kappa(S(\boldsymbol{x}^0, H_1), u_h, f) = \kappa(\tilde{c}, \tilde{w}, \mathcal{L}Q) \tag{5.1}$$

where Q is the $(p+1)$-degree Taylor-series expansion of the exact solution u about $\boldsymbol{x}^0$ and $H_1 = Ch^\alpha$, $0 < \infty < 1$ (see Section 3 and [1]). Hence, for a given Q, the

effectivity index of the estimator can be obtained using the solution of the periodic boundary-value problem (3.7) over the master-cell $\tilde{c}$. Given a class of solutions $\mathcal{U}$, let $\mathcal{Q}$ denote the class of all Taylor-series expansions of functions from $\mathcal{U}$ ($\mathcal{Q}$ is a finite-dimensional space of monomials). For a given mesh-pattern and class of solutions $\mathcal{U}$, we can determine the asymptotic quality of an estimator by computing the asymptotic bounds for the effectivity index

$$C_U = \max_{Q \in \mathcal{Q}} \kappa(\tilde{c}, \tilde{w}, \mathcal{L}Q), \qquad C_L = \max_{Q \in \mathcal{Q}} \kappa(\tilde{c}, \tilde{w}, \mathcal{L}Q) \tag{5.2}$$

The values of C_L, C_U can be computed using numerical optimization. In the numerical study below we considered only *"harmonic" solutions* (by *"harmonic" solution* we mean solution of the homogeneous differential equation or system; when the solution satisfies Laplace's equation it is truly *harmonic*).

Below we analyzed the robustness of the following element-residual (ER) estimators:

1. *Unequilibrated ER* (Est. ER–B) (Eqs. (4.1)-(4.5));
2. *ER with q-order equilibration and (p+1)-degree bubble-space* (Est. ERqB) (Eqs. (4.23)-(4.24))
3. *ER with q-order equilibration and (p+k)-degree polynomial-space* (Est. ERqPp+k) (Eqs. (4.25)-(4.26))
4. *ER with 0th-order equilibration and $(p+k)$-degree polynomial space* (Est. $ER0Pp+k$) (Eqs. (4.25)-(4.26) where $\mathcal{F}_\tau^{EQ,0}$ from eq. (4.37) is employed instead of $\mathcal{F}_\tau^{EQ,q}$ in (4.25)).

The quality of the estimators will be assessed by studying the range of the effectivity-index as a function of the aspect-ratio and the material-orthotropy for the four mesh-patterns of Fig. 4. Based on previous numerical studies [1, 2] we can conjecture that if an estimator is robust with respect to variations of the aspect-ratio and material-orthotropy for these patterns it is also robust for the cases which are encountered in practical computations.

We now present the numerical results.

5.1 Unequilibrated element residual: Sensitivity to the variation of the aspect-ratio

For the estimator ER–B we computed the range of the effectivity index, for the four mesh-patterns and elements of degree p ($2 \leq p \leq 6$), for the aspect-ratios $\frac{1}{1}, \frac{1}{2}, \frac{1}{4}, \frac{1}{8}, \frac{1}{16}$. The results are given in Table 1a-1d. We observe that:

(1) For the Regular pattern the estimator is practically exact for all degrees p.

(2) For the Chevron and the Union-Jack pattern ER–B is an upper estimator and its robustness deteriorates with the aspect-ratio. The worst robustness is obtained for $p = 2$ and aspect-ratio $\frac{1}{16}$, for both the Chevron and the Union-Jack patterns, with robustness index $\mathcal{R} = 5.61$.

(3) For the Criss-Cross pattern ER–B is a lower estimator for aspect-ratio other than $\frac{1}{1}$. The worst robustness for this pattern is obtained for $p = 2$ and aspect-ratio $\frac{1}{16}$ with robustness index $\mathcal{R} = 3.47$.

5.2 The element residual estimator with q-order equilibration and $(p+1)$-degree bubble-space: Sensitivity to the variation of the aspect-ratio

In Tables 2a-2d (resp. 3a-3d) we report the range of the estimator ER1B (resp. ERpB), for the mesh-patterns and elements of degree p, as a function of the aspect-ratio. In Tables 4a-4c we report the same results for the estimator ERp-1B for the Chevron, Union-Jack and Criss-Cross patterns, and in Tables 5a-5b we give results for the estimator ERp-2B for the Union-Jack and Criss-Cross patterns. We observe the following:

(1) Equilibration of order $(p-1)$ dramatically improves the robustness of the estimators which employ the $(p+1)$-degree bubble-space. For the Regular, Chevron and Union-Jack patterns the robustness-index is less than 0.25. For the Criss-Cross pattern the robustness index is less than 0.70.

(2) Comparing Tables 3 and 4 we see that the estimators ERpB and ER(p-1)B give identical results. This can be explained by observing that the p-order corrections along the edges are orthogonal (in the L^2-inner-product) to the edge-restrictions of the $(p+1)$-degree bubble functions.

(3) Similarly, the edge-corrections of degree $q \leq (p-2)$ are orthogonal to the edge-restrictions of the $(p+1)$-degree bubble-funtions. Hence the robustness of the estimators ERqB with $q \leq p-2$, for elements of degree $p \geq 3$, is exactly the same with the robustness of ER–B.

5.3 The element residual estimator ERqPp+1: Sensitivity to the variation of the aspect-ratio

We studied the sensitivity of the range of the effectivity index for the estimator ERqPp+1 with respect to variations of the aspect-ratio. In Tables 6a-6d we report the range of the effectivity index for the estimators ERpPp+1 for the four mesh-patterns. In Table 7 we give the results for the estimator ERp-1Pp+1 for the

Union-Jack and the Criss-Cross pattern and quartic elements ($p = 4$). From the results we observe that:

(1) The estimator ERpPp+1 shows reasonable robustness for all the four mesh-patterns. In the results given in Tables 6a-6d the robustness-index for the estimator does not exceed the value 1.50.

(2) The estimator ERqPp+1 with $q < p$ is not robust. For example the estimator ERp-1Pp+1 for quartic elements in the Criss-Cross pattern has robustness index greater than 14. Greater values of the robustness-index would be obtained if equilibrations of lower-order (i.e. $q < p - 1$) are employed.

5.4 The element residual estimators ERqB and ERqPp+1: Sensitivity to the material-orthotropy

As discussed in [1] and [2], the main-factor which affects the quality of error estimators is the geometry of the mesh. The geometry has to be understood in terms of the values of the coefficients of the differential operator. (For example, let us consider the problem of heat-conduction in a highly orthotropic medium with the principal directions of the material oblique to the mesh. Then, the geometry of the mesh which affects the quality of the estimators can be determined by transforming the geometrical variables so that Laplace operator is obtained in the transformed coordinates (see also [1] for further details).)

To study the robustness of the estimators for orthotropic heat-conduction we considered the class of materials with principal values of orthotropy $1 \leq K_{min} \leq K_{max} \leq 1000$ and orientation θ of one of the principal axes of orthotropy with the fixed coordinate direction; (θ will be called the *grid-material orientation*). Here we varied θ, between 0° and 90°, at increments of 5° and for each grid-material orientation we determined the principal values of orthotropy and the "harmonic" polynomials which correspond to the extrema of the effectivity index. It should be noted that θ corresponds either to the first or the second principal axis depending on the outcome of the optimization. In Table 8 we give the results for cubic elements and all the four mesh-patterns. In Table 8a (resp. Table 8b) we give the sensitivity of the estimator ER1B (resp. ERqB) while in Table 8c (resp. Table 8d) we give the sensitivity of the estimator ER1Pp+1 (resp. ERpPp+1). We observe the following:

(1) The estimator ERpB is the most robust one; for the cases shown in Table 8b the robustness index is less than one.

(2) The estimators ER1Pp+1 and ERpPp+1 are not robust. The robustness index for ER1Pp+1 in Table 8c exceeds 33. By employing p-order order equilibration the robustness is improved somewhat but the value of the robustness index still exceeds 20.

5.5 The estimator ERpPp+∞: The robustness of the optimal version of the estimator

Often in practical applications a conservative estimate of the error is preferred. This has motivated the use of estimators based on the complementary energy-principle. Such estimators can be employed to construct *a global upper-bound of the error in the entire mesh or an upper-bound of the error in the periodic mesh-cell*. Here we will examine the robustness of the optimal version of the element-residual estimator based on the complementary energy-principle, namely the estimator ERpPp+∞ with the optimal equilibration described in Section 4.4. We considered the problem of orthotropic heat-conduction given in Section 5.4 and computed the upper-bound of the estimator ERpPp+2 for the equilibration on the recipe given in [38-39] and the recipe which employs the optimal constants given in Section 4.4. In Table 9 we give the results for the Regular and Criss-Cross pattern with cubic elements. We did not report the lower-bound for the effectivity index which is equal to one in both cases. We computed the estimator by employing only two degrees higher than the order of the element (except in some cases) because we observed that the value of the estimator did not change, for all practical purposes, with a further increase of the order of the local approximation. We observe that:

(1) The robustness of the estimator based on the recipe given in [38-39] is practically the same with the robustness of the estimator based on the optimal constants.

(2) In both cases the robustness is rather poor and the robustness-index exceeds 20.

5.6 The robustness of the estimator ER0Pp+k: Sensitivity to the variation of the aspect-ratio

Here we studied the robustness of the estimator ER0Pp+3 for the Laplace equation by computing the sensitivity of the estimator to the variation of the aspect-ratio for the Criss-Cross pattern and cubic elements ($p = 3$). In Table 10 we report the range of the effectivity index. We observe that:

(1) This is an upper estimator.

(2) This estimator ER0Pp+3 is not robust. For aspect-ratio $\frac{1}{16}$ the robustness index exceeds 17.

5.7 The robustness of the estimators ERqB, ERqPp + k for the isotropic elasticity problem: Sensitivity to the variation of the aspect-ratio

Here we studied the robustness of the estimators ER1B, ERpB, ER1Pp+3, ERpPp+3 for the elasticity problem by computing their sensitivity to the variation of the aspect-ratio. In Tables 11a-11d (resp. Tables 12a-12d) we give the values of C_L, C_U for the estimator ER1B (resp. ERpB), for $p = 2, 3, 4$. In Table 13a (resp. Table 13b) we give the values of C_L, C_U for ER1Pp+3 (resp. ERpPp+3) for $p = 3$. All the results given here were obtained for Poisson's ratio equal to 0.3; (from the results given in [1-2] we expect a small variation of the robustness with the value of Poisson's ratio). We observe that:

(1) We can draw the same conclusions about the estimators as in the case of isotropic heat-conduction.

(2) The estimator ERpB is the most robust and its robustness-index does not exceed 1.

(3) The error estimator ERpPp+3 (which is practically the estimator based on the complementary energy-principle) shows poor robustness and its robustness-index exceeds 40.

(4) The error estimator ER1Pp+3 in the case of the Criss-Cross pattern with aspect-ratio $\frac{1}{16}$ has a robustness-index exceeding 680.

5.8 The estimator ERpPp + ∞ for the elasticity problem: The robustness of the optimal version of the estimator

As in Section 5.5 we studied the robustness of the optimal version of the estimator ERpPp+∞ for the elasticity problem. Here we studied the robustness with respect to variations of the aspect-ratio. In Table 14 we give the values of C_L, C_U for the optimal version estimator ERpPp+3 (which is practically the same as ERpPp+∞) for the four mesh-patterns and cubic elements. We observe that:

(1) By comparing the results of Tables 14 and 13b we see that the optimal version of the estimator is substantially more robust than the version based on the recipe given in [38-39].

(2) The robustness of the optimal version of the estimator ERpPp+∞ is poor. The robustness-index for this estimator for the Criss-Cross pattern with aspect ratio $\frac{1}{16}$ exceeds 20.

5.9 The estimators ER–B, ER1B, ERpB for meshes of square-elements with local refinements: Sensitivity to the material-orthotropy for the three element types

We also studied the robustness of the estimators ER–B, ER1B and ERpB for meshes of square-elements with local refinements. Here we are interested in the robustness of the estimators for the three element-types, namely the tensor-product (eq. (2.11)), Serendipity (eq. (2.12)) and intermediate (eq. (2.13)) elements.

We now briefly describe the construction of the edgewise polynomial corrections for meshes of square elements with refinements. Let us consider the mesh-patch associated with vertex X as shown in Fig. 5. The element τ_i^X ($i = 1, 2, \ldots, 6$) and the edges ϵ_j^X ($j = 1, 2, \ldots, 8$) are also shown in Fig. 5. Here an edge is defined as the intersection of the boundary of two elements therefore a side of a square element may consist of two edges.

We first define the linear corrections of the form

$$\theta^\epsilon = (\theta^{\epsilon,1}\bar{\psi}_1^\epsilon + \theta^{\epsilon,2}\bar{\psi}_2^\epsilon), \qquad \int_\epsilon \bar{\psi}_i^\epsilon \lambda_j = \delta_{ij} \qquad i, j = 1, 2$$

Here λ_j are the linear shape functions corresponding to the two end nodes of the edge. If the edge ϵ does not have any irregular end-points then $\bar{\psi}_i^\epsilon \equiv \psi_i^\epsilon$, where ψ_i^ϵ is given in eq. (4.15). If one of the end-points of the edge is an irregular node, as shown in Fig. 5b, we have:

$$\bar{\psi}_1^{\epsilon_1} = \frac{1}{|\epsilon_1|}(4\lambda_1 - 8\lambda_2), \quad \bar{\psi}_2^{\epsilon_1} = \frac{1}{|\epsilon_1|}(-\frac{2}{3}\lambda_1 + \frac{7}{3}\lambda_2)$$

for the edge ϵ_1 which has its right-end-point at the irregular node (see Fig. 5b);

$$\bar{\psi}_1^{\epsilon_2} = \frac{1}{|\epsilon_2|}(\frac{7}{3}\lambda_1 - \frac{2}{3}\lambda_2), \quad \bar{\psi}_2^{\epsilon_2} = \frac{1}{|\epsilon_2|}(-8\lambda_1 + 4\lambda_2)$$

for the edge ϵ_2 which has its left-end-point at the irregular node (see Fig. 5b). Here λ_1, λ_2 are the linear shape-functions corresponding to the end-points of the segment $\bar{\epsilon}_1 \bigcup \bar{\epsilon}_2$, as shown in Fig. 5b. Following the similar steps given in Section 4.2, we get the following system of equations:

$$\begin{bmatrix} -1 & 1 & 1 & 0 & 0 & 0 & 0 & 0 \\ 0 & -1 & 0 & 1 & 0 & 0 & -1 & 1 \\ 0 & 0 & -1 & 0 & 0 & 0 & 1 & 0 \\ 0 & 0 & 0 & 0 & 1 & 0 & 0 & -1 \\ 0 & 0 & 0 & -1 & -1 & 1 & 0 & 0 \\ 1 & 0 & 0 & 0 & 0 & -1 & 0 & 0 \end{bmatrix} \begin{Bmatrix} \theta^{\epsilon_1^X,\nu(\epsilon_1^X)} \\ \theta^{\epsilon_2^X,\nu(\epsilon_2^X)} \\ \theta^{\epsilon_3^X,\nu(\epsilon_3^X)} \\ \theta^{\epsilon_4^X,\nu(\epsilon_4^X)} \\ \theta^{\epsilon_5^X,\nu(\epsilon_5^X)} \\ \theta^{\epsilon_6^X,\nu(\epsilon_6^X)} \\ \theta^{\epsilon_7^X,\nu(\epsilon_7^X)} \\ \theta^{\epsilon_8^X,\nu(\epsilon_8^X)} \end{Bmatrix} = \begin{Bmatrix} -\mathcal{F}_{\tau_1^X}(\phi_X) \\ -\mathcal{F}_{\tau_2^X}(\phi_X) \\ -\mathcal{F}_{\tau_3^X}(\phi_X) \\ -\mathcal{F}_{\tau_4^X}(\phi_X) \\ -\mathcal{F}_{\tau_5^X}(\phi_X) \\ -\mathcal{F}_{\tau_6^X}(\phi_X) \end{Bmatrix}$$

We solve for $\theta^{\epsilon_k,\nu(\epsilon_k)}$ by minimizing the expansion in (4.20) with $w_k = \frac{1}{|\epsilon_k^X|}$.

We now outline the steps involved to compute higher-order corrections. In order to determine the higher-order corrections, we define the conjugate basis $\{\bar{\psi}_i\}$ over each edge as

$$\int_\epsilon \bar{\psi}_i \phi_{\epsilon,j} := \begin{cases} 0, & \text{if } j < i \\ 1, & \text{if } j = i \end{cases}$$

where $\phi_{\epsilon,i}$, $i = 3, \ldots, (q+1)$ denote the basis functions which do not vanish on edge ϵ. We obtain the higher-order corrections $\theta^{\epsilon,j}$, $j = 3, \ldots, (q+1)$ using

$$\theta^{\epsilon,i} = -\mathcal{F}_{\tau_{\text{out}}}(\phi_{\epsilon,i}) - \sum_{j=1}^{i-1} \theta^{\epsilon,j} \int_\epsilon \bar{\psi}_j \phi_{\epsilon,i}\,, \qquad \epsilon \subseteq \partial\tau_{\text{out}}$$

Note that the integrals on the right-hand side can be computed explicitly on the master element $\hat{\epsilon} = [-1, 1]$, therefore the cost of computing the higher order terms $\theta^{\epsilon,i}$, $i = 3, \ldots, (q+1)$ is negligible.

We studied the robustness of the estimators for solutions of the equation of orthotropic heat-conduction, for the general class of solutions, in the mesh-cells shown in Figs. 6a and 6b. We computed the range of the effectivity index as a function of the grid-material orientation for orthotropy $\frac{K_{max}}{K_{min}} = 100$. In Tables 15 and 16 we give the results for the three element types, for the mesh-cell at the mesh-interface (shown in Fig. 6a), for cubic and quartic elements, respectively. In

Table 17a (resp. Table 17b) we give the results for tensor-product (resp. Serendipity) elements of degree 5, for the mesh-cell at the mesh-interface. In Tables 18a (resp. Table 18b) we give the results for the periodic mesh-cell with two-levels of refinements shown in Fig. 6b for tensor-product (resp. Serendipity) elements of degree 3. We observe the following:

(1) The estimators ER–B and ER1B have practically the same range of effectivity index for the three element-types. Hence linear equilibration is not effective for elements of degree $p \geq 3$.

(2) The estimator ERpB is very robust; for the cases shown in Tables 15-18, its robustness-index does not exceed 0.4.

(3) The largest values of the robustness-index (for a given element-degree p) for all the estimators are observed to be the largest for the serendipity elements. The robustness of the estimators for the tensor-product and intermediate element-types is practically the same.

5.10 Analysis of the effect of the order of equilibration on the value of the effectivity index

In order to analyze further the effect of higher-order equilibration on the value of the effectivity index we noted that

$$\kappa^2(c(\boldsymbol{x}^0,h),u_h,f) = 1 + \frac{\sum_{i=1}^{4} |||\hat{e}_{\tau_i} - e_h|||^2_{\tau_i}}{\sum_{i=1}^{4} |||e_h|||^2_{\tau_i}} + 2\,\frac{\sum_{i=1}^{4} b_\tau(\hat{e}_{\tau_i} - e_h, e_h)}{\sum_{i=1}^{4} |||e_h|||^2_{\tau_i}} \tag{5.3}$$

and computed the value of the second- and the third-term on the right-hand side of (5.3) for ER1B, ERpB, ER1Pp+3, ERpPp+3. In Table 19 we give the values for the Criss-Cross pattern with aspect-ratio $\frac{1}{4}$. We solved Laplace's equation with quartic elements to approximate the harmonic monomials $Q_1(x_1,x_2) = \mathcal{R}e((x_1 + ix_2)^5)$, $Q_2(x_1,x_2) = \mathcal{J}m((x_1+ix_2)^5)$. We observe the following

(1) The robust versions of the estimators are obtained because *the higher-order equilibration causes cancellation between the second and the third-term in the expansion* (5.3).

(2) The term $\left[\frac{\sum_{i=1}^{4} |||\hat{e}_{\tau_i} - e_h|||^2_{\tau_i}}{\sum_{i=1}^{4} |||e_h|||^2_{\tau_i}}\right]^{\frac{1}{2}}$ is the value of the relative error in the error-indicator functions in the mesh-pattern. Note that *even with p-order equilibration this relative error is more than 100%* for all the cases listed in Table 19.

5.11 The equilibrated patch-residual error estimator: Robustness of the various versions of the estimator

In order to construct residual estimator which are more robust than the element-residual estimator described and analyzed above. Let us assume that we are interested to estimate the error in the mesh-cell $T(\boldsymbol{x}^0, h)$. Then we consider the following *patch-residual* problem over the mesh-cell $T(\boldsymbol{x}^0, 2h)$:

Find $\hat{e} \in S_h^{p+k}(T(\boldsymbol{x}^0, 2h))$ such that

$$\sum_{\tau \in T(\boldsymbol{x}^0, 2h)} b_\tau(\hat{e}, v) = \sum \mathcal{F}_\tau^{EQ}(v) \qquad \forall\, v \in S_h^{p+k}(T(\boldsymbol{x}^0, 2h)) \tag{5.4}$$

Here $S_h^{p+k}(T(\boldsymbol{x}^0, 2h))$ denotes the elementwise $(p+k)$-degree polynomial space over the mesh-cell $T(\boldsymbol{x}^0, 2h)$. The error estimator in the mesh-cell $T(\boldsymbol{x}^0, h)$ is given by:

$$\mathcal{E}_{T(\boldsymbol{x}^0, h)} := \sqrt{\sum_{\tau \in T(\boldsymbol{x}^0, h)} |||\hat{e}|||_\tau^2} \tag{5.5}$$

As an example we considered $T(\boldsymbol{x}^0, h)$ to be the mesh-cell for the Criss-Cross pattern shown in Fig. 4d. We solved the problem of orthotropic heat-conduction (with $1 \leq K_{min} \leq K_{max} \leq 1000$ as described above) with cubic elements. We computed the error-indicator function (5.4) by letting $k = 1$ and by employing linear and p-order equilibration. From the results, which are are given in Table 20, we observe the following:

(1) The patch-residual estimators are much more robust than the corresponding versions of the element-residual estimators. For example when p-order equilibration is employed the robustness-index for ERpPp+1 for cubic elements in the Criss-Cross pattern is greater than 10 while the robustness-index for the corresponding patch-residual estimator does not exceed 0.5.

(2) The patch-residual estimator with p-order equilibration is more robust than the corresponding estimator with linear equilibration. For example in Table 20 the robustness-index of the patch-residual estimator with linear equilibration is greater than 2.

6 Conclusions

We presented a model study of the element-residual estimators in the interior of patchwise uniform meshes. The results of this study are indicative of the expected performance of these estimators in the interior of general grids. From the results presented the following conclusions can be drawn:

(1) Higher-order equilibration substantially improves the robustness of the element-residual estimators.

(2) The estimator based on the complementary energy-principle is not robust (even in its optimal version) with respect to variations of the aspect-ratio or the material-orthotropy.

(3) The estimator ERpB which employs p-order equilibration and $(p+1)$-degree bubble-type approximation of the solution of the local problem is the most robust.

(4) The robustness of the element residual estimators can be further improved by constructing patch-residual estimators by assembling the element-residual problems in a patch. By employing p-order equilibration to set the boundary-conditions for the patch-residual problem we can obtain very robust estimator even in the cases of extreme material-orthotropy.

References

[1] I. Babuška, T. Strouboulis and C.S. Upadhyay, A model study of the quality of a posteriori error estimators for linear elliptic problems: Error estimation in the interior of patchwise uniform grids of triangles, Comput. Methods Appl. Mech. Engrg. (1994), in press.

[2] I. Babuška, T. Strouboulis, C.S. Upadhyay, S.K. Gangaraj and K. Copps, Validation of a posteriori error estimators by numerical approach, Internat. J. Numer. Methods Engrg. 37 (1994), in press.

[3] I. Babuška, R. Durán and R. Rodriguez, Analysis of the efficiency of an a-posteriori error estimator for linear triangular finite elements, SIAM J. Numer. Anal. 29 (4) (1992) 947-964.

[4] I. Babuška, L. Plank and R. Rodriguez, Quality assessment of the a-posteriori error estimation in finite elements, Finite Elements in Analysis and Design 11 (1992) 285-306.

[5] I. Babuška, L. Plank and R. Rodriguez, Basic problems of a-posteriori error estimation, Comput. Methods Appl. Mech. Engrg. 101 (1992) 97-112.

[6] I. Babuška and W.C. Rheinboldt, Error estimates for adaptive finite element computations, SIAM J. Numer. Anal. 15 (4) (1978) 736-754.

[7] I. Babuška and W.C. Rheinboldt, A-posteriori error estimates for the finite element method, Internat. J. Numer. Methods Engrg. 12 (1978) 1597-1615.

[8] I. Babuška and W.C. Rheinboldt, Reliable error estimation and mesh adaptation for the finite element method, in: J.T. Oden, ed., Computational Methods in Nonlinear Mechanics (North Holland, Amsterdam, 1980) 67-108.

[9] I. Babuška and W.C. Rheinboldt, A posteriori error analysis of finite element solutions for one-dimensional problems, SIAM J. Numer. Anal. 18 (3) (1981) 565-589.

[10] I. Babuška and A. Miller, A-posteriori error estimates and adaptive techniques for the finite element method, Technical Note BN-968, Institute for Physical Science and Technology, University of Maryland, 1981.

[11] R.E. Bank and A. Weiser, Some a posteriori error estimators for elliptic partial differential equations, Math. Comp. 44 (1985) 283-301.

[12] I. Babuška and A. Miller, A feedback finite element method with a posteriori error estimation: Part I. The finite element method and some basic properties of the a posteriori error estimator, Comput. Methods Appl. Mech. Engrg. 61 (1987) 1-40.

[13] I. Babuška and D. Yu, Asymptotically exact a posteriori error estimator for biquadratic elements, Finite Elements in Analysis and Design 3 (1987) 341-354.

[14] J.T. Oden, L. Demkowicz, W. Rachowicz and T.A. Westermann, Toward a universal h-p adaptive finite element strategy: Part 2, A Posteriori Error Estimates, Comput. Methods Appl. Mech. Engrg. 77 (1989) 113-180.

[15] T.A. Westermann, A Posteriori Estimation of Errors in hp finite element methods for linear elliptic boundary value problems, M.Sc. Thesis, The University of Texas at Austin, Austin, Texas, 1989.

[16] R. Verfürth, A posteriori error estimators for the Stokes equation, Numer. Math. 55 (1989) 309-325.

[17] R. Verfürth, A posteriori error estimation and adaptive mesh refinement techniques, J. Comput. Appl. Math., (1993), to appear.

[18] J. Baranger and H. El-Amri, Estimateurs a posteriori d' erreur pour le calcul adaptatif d' ecoulements quasi-newtoniens, RAIRO Math. Model. Numer. Anal. 25 (1) (1991) 31-48.

[19] M. Ainsworth and A. Craig, A posteriori error estimators in the finite element method, Numer. Math. 60 (1992) 429-463.

[20] M. Ainsworth and J.T. Oden, A unified approach to a-posteriori error estimation using element residual methods, Numer. Math. 65 (1993) 23-50.

[21] R. Durán and R. Rodriguez, On the asymptotic exactness of Bank-Weiser's estimator, Numer. Math. 62 (1992) 297-303.

[22] T. Strouboulis and K.A. Haque, Recent experiences with error estimation and adaptivity, Part I: Review of error estimators for scalar elliptic problems, Comput. Methods Appl. Mech. Engrg. 97 (1992) 399-436.

[23] T. Strouboulis and K.A. Haque, Recent experiences with error estimation and adaptivity, Part II: Error estimation for h-adaptive approximations on grids of triangles and quadrilaterals, Comput. Methods Appl. Mech. Engrg. 100 (1992) 359-430.

[24] M. Ainsworth and J. .T. Oden, A procedure for a posteriori error estimation for h-p finite element methods, Comput. Methods Appl. Mech. Engrg. 101 (1992) 73-96.

[25] R.E. Bank and R.K. Smith, A posteriori error estimates based on hierarchical bases, SIAM J. Numer. Anal. 30 (1993) 921-935.

[26] R. Verfürth, A review of a-posteriori error estimation and adaptive mesh-refinement techniques, Technical Report, Institüt für Angewandte Mathematik der Universität Zürich, 1993.

[27] W. Práger and J.L. Synge, Approximations in elasticity based on the concept of the function space, Quart. Appl. Math. 5 (3) (1947) 241-269.

[28] J.L. Synge, The Hypercircle in Mathematical Physics (Cambridge at the University Press, Cambridge, Great Britain, 1957).

[29] J.P. Aubin and H.G. Burchard, Some aspects of the method of the hypercircle applied to elliptic variational problems, in: SYNSPADE 1970, B. Hubbard (ed.) (Academic Press, New York, 1971) 1-67.

[30] J. Vacek, Dual variational principles for an elliptic partial differential equation, Aplik. Mat. 21 (1976) 5-26.

[31] P. Ladeveze, Comparaison de modeles de milieux continus, These, Universite P. et M. Curie, Paris, 1975.

[32] P. Ladeveze, Nouvelle procedure d' estimation d'erreurr relative a la methode des elements finis et applications, Journées Eléments Finis, Rennes, 1977.

[33] P. Ladeveze and D. Leguillon, Error estimate procedure in the finite element method and applications, SIAM J. Numer. Anal. 20 (3) (1983) 485-509.

[34] D.W. Kelly, The self-equilibration of residuals and complementary a posteriori error estimates in the finite element method, Internat. J. Numer. Methods Engrg. 20 (1984) 1491-1506.

[35] D.W. Kelly, R.J. Mills, J.A. Reizes and A.D. Miller, Aposteriori estimates of the solution error caused by discretization in the finite element, finite difference and boundary element methods, Internat. J. Numer. Methods Engrg. 24 (1987) 1921-1939.

[36] D.W. Kelly and J.D. Isles, A procedure for a posteriori error analysis for the finite element method which contains a bounding measure, Computers & Structures 31 (1989) 63-71.

[37] D.W. Kelly and J.D. Isles, Procedures for residual equilibration and local error estimation in the finite element method, Commun. Appl. Numer. Methods 5 (1989) 497-505.

[38] P. Rougeot, Sur le controle de la qualite des maillages elements finis, These de Doctorat de l'Universite Paris 6, Cachan, France, June 1989.

[39] P. Ladeveze, J.P. Pelle and P. Rougeot, Error estimation and mesh optimization for classical finite elements, Engineering Computations 8 (1991) 69-80.

[40] P. Ladeveze, P. Marin, J.P. Pelle and G.L. Gastine, Accuracy and optimal meshes in finite element computation for nearly incompressible materials, Comput. Methods Appl. Mech. Engrg. 94 (1992) 303-315.

[41] P. Coorevits, Maillage adaptatif anisotrope: Application aux problems de dynamique, Thése de Doctorat de l'Ecole Normale Superieure de Cachan, Paris, France, January 1993.

[42] J.D. Yang, D.W. Kelly and J.D. Isles, A posteriori pointwise upper bound error estimates in the finite element method, Internat. J. Methods Engrg. 36 (1993) 1279-1298.

[43] M. Ainsworth and J.T. Oden, A posteriori error estimators for second order elliptic systems Part 1. Theoretical foundations and a posteriori error analysis, Comput. Math. Appl. 25 (1993) 101-113.

[44] M. Ainsworth and J.T. Oden, A posteriori error estimatots for second order elliptic systems. Part 2. An optimal order process for calculating self-equilibrating fluxes, Comput. Math. Appl. 26 (1993) 75-87.

[45] J.T. Oden and H. Brauchli, On the calculation of consistent stress distributions in the finite element approximations, Internat. J. Numer. Methods Engrg. 3 (1971) 317-325.

[46] O.C. Zienkiewicz and J.Z. Zhu, A simple error estimator and adaptive procedure for practical engineering analysis, Internat. J. Numer. Methods Engrg. 24 (1987) 337-357.

[47] E. Rank and O.C. Zienkiewicz, A simple error estimator in the finite element method, Comm. Appl. Numer. Methods 3 (1987) 243-249.

[48] W. Rachowicz and J.T. Oden, On the accuracy and convergence of conjugate flux approximations, Internat. J. Numer. Methods for Partial Differential Equations 5 (1989) 143-156.

[49] M. Ainsworth, J.Z. Zhu, A.W. Craig and O.C. Zienkiewicz, Analysis of the Zienkiewicz-Zhu a posteriori error estimator in the finite element method, Internat. J. Numer. Methods Engrg. 28 (1989) 2161-2174.

[50] M.S. Shephard, Q. Niu and P.L. Baehmann, Some results using stress projectors for error indication in: J.E. Flaherty, P.J. Paslow, M.S. Shephard, J.D. Vasilakis, eds., Adaptive Methods for Partial Differential Equations (SIAM, Philadelphia, 1989) 83-99.

[51] J.Z. Zhu and O.C. Zienkiewicz, Superconvergence recovery technique and a posteriori error estimators, Internat. J. Numer. Methods Engrg. 30 (1990) 1321-1339.

[52] O.C. Zienkiewicz and J.Z. Zhu, The superconvergence patch recovery and a posteriori error estimates. Part 1: The recovery technique, Internat. J. Numer. Methods Engrg. 33 (1992) 1331-1364.

[53] O.C. Zienkiewicz and J.Z. Zhu, The superconvergence patch recovery and a posteriori error estimates. Part 2: Error estimates and adaptivity, Internat. J. Numer. Methods Engrg. 33 (1992) 1365-1382.

[54] O.C. Zienkiewicz and J.Z. Zhu, The superconvergence patch recovery (SPR) and adaptive finite element refinement, Comput. Methods Appl. Mech. Engrg. 101 (1992) 207-224.

[55] I. Babuška and R. Rodriguez, The problem of the selection of an a-posteriori error indicator based on smoothening techniques, Internat. J. Numer. Methods Engrg. 36 (1993) 539-567.

[56] R. Durán, M.A. Muschietti and R. Rodriguez, On the asymptotic exactness of the error estimators for linear triangular elements, Numer. Math. 59 (1991) 107-127.

[57] R. Durán, M.A. Muschietti and R. Rodriguez, Asymptotically exact error estimators for rectangular finite elements, SIAM J. Numer. Anal. 29 (1) (1992) 78-88.

[58] O.C. Zienkiewicz, J.Z. Zhu and J. Wu, Superconvergent patch recovery techniques. Some further tests, Comm. Numer. Methods Engrg. 9 (1993) 251-258.

[59] J.Z. Zhu, Further tests on the derivative recovery technique and a posteriori error estimator, in Finite Elements in the 90's, E. Oñate, J. Periaux, A. Samuelson, Eds., Springer-Verlag/CIMNE, Barcelona (1991) 594-604.

[60] N.E. Wiberg and F. Abdulwahab, A posteriori error estimation based on superconvergent derivatives and equilibrium, Internat. J. Numer. Methods Engrg. 36 (1993) 2703-2724.

[61] A. Samuelson, N.E. Wiberg and L.F. Zeng, The effectivity of the Zienkiewicz-Zhu error estimate and two 2D adaptive mesh generators, Commun. Num. Methods Engrg. 9 (1993) 687-699.

[62] T. Blacker and T. Belytschko, Superconvergent patch recovery with equilibrium and conjoint interpolant enhancements, Internat. J. Numer. Methods Engrg. 37 (1994) 517-536.

[63] R. Rodriguez, Some remarks on Zienkiewicz-Zhu estimator, Internat. J. Numer. Methods in PDEs (1994), to appear.

[64] K. Eriksson and C. Johnson, An adaptive finite element method for linear elliptic problems, Math. Comp. 50 (1988) 361-383.

[65] C. Johnson and P. Hansbo, Adaptive finite element methods in computational mechanics, Comput. Methods Appl. Mech. Engrg. 101 (1992) 143-181.

[66] I. Babuška and A.K. Aziz, Foundations of the finite element method, in: A.K. Aziz, ed., The Mathematical Foundations of the Finite Element Method with Applications to Partial Differential Equations (Academic Press, New York, 1972) 5-359.

[67] P.G. Ciarlet, Basic error estimates for elliptic problems, in: P.G. Ciarlet and J.L. Lions, eds., Handbook of Numerical Analysis, Vol. II (North-Holland, Amsterdam, 1991) 17-351.

[68] I. Babuška and J.T. Oden, Benchmark computation: What is its purpose and meaning, IACM Bulletin 7(4) (1992) 83-84.

[69] L.B. Wahlbin, Local behavior in finite element methods, in: P.G. Ciarlet and J.L. Lions, eds., Handbook of Numerical Analysis, Vol. II (North-Holland, Amsterdam, 1991) 357-522.

[70] S.G. Lekhnitskii, Theory of Elasticity of an Anisotropic Elastic Body, (Holden-Day Inc., San Francisco, 1963).

[71] I. Babuška, B.A. Szabo and R.L. Actis, Hierarchic models for laminated composites, Internat. J. Numer. Methods Engrg. 33 (1992) 503-535.

[72] B.A. Szabo and I. Babuška, Finite Element Analysis, John Wiley & Sons, Inc., New York, 1991.

[73] C. Johnson and B. Mercier, Some equilibrium finite element methods for two-dimen-sional elasticity problems, Numer. Math. 30 (1978) 103-116.

[74] I. Babuška, T. Strouboulis, A. Mathur and C.S. Upadhyay, Pollution error in the h-version of the finite-element method and the local quality of a-posteriori error estimators, Finite Elements in Analysis and Design (1994), in press.

[75] I. Babuška, T. Strouboulis, C.S. Upadhyay and S.K. Gangaraj, Study of superconvergence by a computer-based approach. Superconvergence of the gradient in finite element solutions of Laplace's and Poisson's equations, Technical Note BN-1155, Institute for Physical Science and Technology, University of Maryland, College Park, November 1993.

[76] L. Demkowicz, J.T. Oden, W. Rachowicz and O. Hardy, Toward a universal h-p adaptive finite element strategy, Part 1: Constrained approximation and data structure, Comput. Methods Appl. Mech. Engrg. 77 (1989) 79-112.

Unequilibrated ER with (p+1)-degree bubble-space										
Regular Pattern										
Aspect Ratio	$p=2$		$p=3$		$p=4$		$p=5$		$p=6$	
	C_L	C_U	C_L	C_U	C_L	C_U	C_L	C_U	C_L	C_U
$\frac{1}{1}$	1.000	1.000	0.948	1.000	0.985	0.986	0.984	0.999	0.995	0.996
$\frac{1}{2}$	1.000	1.000	0.972	1.000	0.994	0.995	0.986	1.000	0.992	0.999
$\frac{1}{4}$	1.000	1.000	0.992	1.000	0.999	0.999	0.995	1.000	0.998	1.000
$\frac{1}{8}$	1.000	1.000	0.998	1.000	1.000	1.000	0.999	1.000	1.000	1.000
$\frac{1}{16}$	1.000	1.000	1.000	1.000	1.000	1.000	1.000	1.000	1.000	1.000

Table 1a. Unequilibrated ER with $(p+1)$-degree bubble-space: Laplace's equation. Range of the effectivity index as a function of the aspect-ratio for the Regular pattern.

Unequilibrated ER with $(p+1)$-degree bubble-space										
Chevron Pattern										
Aspect Ratio	$p=2$		$p=3$		$p=4$		$p=5$		$p=6$	
	C_L	C_U	C_L	C_U	C_L	C_U	C_L	C_U	C_L	C_U
$\frac{1}{1}$	1.000	1.049	0.948	1.017	0.986	0.995	0.984	1.003	0.995	0.997
$\frac{1}{2}$	1.000	1.281	0.972	1.160	0.994	1.112	0.986	1.080	0.992	1.059
$\frac{1}{4}$	1.000	1.922	0.992	1.568	0.999	1.414	0.995	1.316	0.998	1.259
$\frac{1}{8}$	1.000	3.423	0.998	2.551	1.000	2.116	0.999	1.854	1.000	1.692
$\frac{1}{16}$	1.000	6.612	1.000	4.746	1.000	3.755	1.000	3.143	1.000	2.737

Table 1b. Unequilibrated ER with $(p+1)$-degree bubble-space: Laplace's equation. Range of the effectivity index as a function of the aspect-ratio for the Chevron pattern.

Unequilibrated ER with (p+1)-degree bubble-space										
Union-Jack Pattern										
Aspect Ratio	$p=2$		$p=3$		$p=4$		$p=5$		$p=6$	
	C_L	C_U	C_L	C_U	C_L	C_U	C_L	C_U	C_L	C_U
$\frac{1}{1}$	1.049	1.049	0.948	1.033	0.995	0.995	0.984	1.007	0.997	0.997
$\frac{1}{2}$	1.003	1.281	0.972	1.160	0.994	1.112	0.986	1.080	0.992	1.059
$\frac{1}{4}$	1.001	1.922	0.992	1.568	0.999	1.414	0.995	1.316	0.998	1.259
$\frac{1}{8}$	1.000	3.423	0.998	2.551	1.000	2.116	0.999	1.854	1.000	1.692
$\frac{1}{16}$	1.000	6.612	1.000	4.746	1.000	3.755	1.000	3.143	1.000	2.737

Table 1c. Unequilibrated ER with $(p+1)$-degree bubble-space: Laplace's equation. Range of the effectivity index as a function of the aspect-ratio for the Union-Jack pattern.

Unequilibrated ER with (p+1)-degree bubble-space										
Criss-Cross Pattern										
Aspect Ratio	$p=2$		$p=3$		$p=4$		$p=5$		$p=6$	
	C_L	C_U	C_L	C_U	C_L	C_U	C_L	C_U	C_L	C_U
$\frac{1}{1}$	1.049	1.049	0.948	1.033	0.995	0.995	0.984	1.007	0.997	0.997
$\frac{1}{2}$	0.891	0.959	0.894	0.930	0.897	0.944	0.899	0.950	0.938	0.9[illegible]
$\frac{1}{4}$	0.570	0.906	0.702	0.841	0.692	0.848	0.707	0.869	0.757	0.894
$\frac{1}{8}$	0.339	0.894	0.512	0.816	0.469	0.812	0.549	0.829	0.536	0.855
$\frac{1}{16}$	0.230	0.891	0.40[illegible]	0.810	0.323	0.803	0.493	0.818	0.377	0.841

Table 1d. Unequilibrated ER with $(p+1)$-degree bubble-space: Laplace's equation. Range of the effectivity index as a function of the aspect-ratio for the Criss-Cross pattern.

ER with linear equilibration and $(p+1)$-degree bubble-space										
Regular Pattern										
Aspect Ratio	$p=2$		$p=3$		$p=4$		$p=5$		$p=6$	
	C_L	C_U	C_L	C_U	C_L	C_U	C_L	C_U	C_L	C_U
$\frac{1}{1}$	1.000	1.000	0.948	1.000	0.985	0.985	0.984	0.999	0.996	0.996
$\frac{1}{2}$	1.000	1.000	0.972	1.000	0.994	0.995	0.986	1.000	0.992	0.999
$\frac{1}{4}$	1.000	1.000	0.992	1.000	0.999	0.999	0.995	1.000	0.998	1.000
$\frac{1}{8}$	1.000	1.000	0.998	1.000	1.000	1.000	0.999	1.000	1.000	1.000
$\frac{1}{16}$	1.000	1.000	0.999	1.000	1.000	1.000	1.000	1.000	1.000	1.000

Table 2a. ER with linear equilibration and $(p+1)$-degree bubble-space: Laplace's equation Range of the effectivity index as a function of the aspect-ratio for the Regular pattern.

ER with linear equilibration and $(p+1)$-degree bubble-space										
Chevron Pattern										
Aspect Ratio	$p=2$		$p=3$		$p=4$		$p=5$		$p=6$	
	C_L	C_U	C_L	C_U	C_L	C_U	C_L	C_U	C_L	C_U
$\frac{1}{1}$	1.000	1.008	0.948	1.017	0.986	0.995	0.984	1.003	0.995	0.997
$\frac{1}{2}$	1.000	1.009	0.972	1.160	0.994	1.112	0.986	1.080	0.992	1.059
$\frac{1}{4}$	1.000	1.004	0.992	1.568	0.999	1.414	0.995	1.316	0.998	1.259
$\frac{1}{8}$	1.000	1.001	0.998	2.551	1.000	2.116	0.999	1.854	1.000	1.692
$\frac{1}{16}$	1.000	1.000	1.000	4.746	1.000	3.755	1.000	3.143	1.000	2.737

Table 2b. ER with linear equilibration and $(p+1)$-degree bubble-space: Laplace's equation. Range of the effectivity index as a function of the aspect-ratio for the Chevron pattern.

ER with linear equilibration and $(p+1)$-degree bubble-space										
Union-Jack Pattern										
Aspect Ratio	$p=2$		$p=3$		$p=4$		$p=5$		$p=6$	
	C_L	C_U	C_L	C_U	C_L	C_U	C_L	C_U	C_L	C_U
$\frac{1}{1}$	1.000	1.000	0.948	1.033	0.995	0.995	0.984	1.007	0.997	0.997
$\frac{1}{2}$	1.000	1.000	0.972	1.160	0.994	1.112	0.986	1.080	0.992	1.059
$\frac{1}{4}$	1.000	1.000	0.992	1.568	0.999	1.414	0.995	1.316	0.998	1.259
$\frac{1}{8}$	1.000	1.000	0.998	2.551	1.000	2.116	0.999	1.854	1.000	1.692
$\frac{1}{16}$	1.000	1.000	1.000	4.746	1.000	3.755	1.000	3.143	1.000	2.737

Table 2c. ER with linear equilibration and $(p+1)$-degree bubble-space: Laplace's equation. Range of the effectivity index as a function of the aspect-ratio for the Union-Jack pattern.

ER with linear equilibrationn and $(p+1)$-degree bubble-space										
Criss-Cross Pattern										
Aspect Ratio	$p=2$		$p=3$		$p=4$		$p=5$		$p=6$	
	C_L	C_U	C_L	C_U	C_L	C_U	C_L	C_U	C_L	C_U
$\frac{1}{1}$	1.000	1.000	0.948	1.033	0.995	0.995	0.984	1.007	0.997	0.997
$\frac{1}{2}$	0.922	0.977	0.894	0.930	0.897	0.944	0.899	0.950	0.938	0.958
$\frac{1}{4}$	0.796	0.985	0.702	0.841	0.692	0.848	0.707	0.869	0.757	0.894
$\frac{1}{8}$	0.733	0.995	0.512	0.816	0.469	0.812	0.549	0.829	0.536	0.855
$\frac{1}{16}$	0.714	0.999	0.406	0.810	0.323	0.803	0.493	0.818	0.377	0.841

Table 2d. ER with linear equilibration and $(p+1)$-degree bubble-space: Laplace's equation. Range of the effectivity index as a function of the aspect-ratio for the Criss-Cross pattern.

ER with p-order equilibration and $(p+1)$-degree bubble-space										
Regular Pattern										
Aspect Ratio	$p=2$		$p=3$		$p=4$		$p=5$		$p=6$	
	C_L	C_U	C_L	C_U	C_L	C_U	C_L	C_U	C_L	C_U
$\frac{1}{1}$	1.000	1.000	0.948	1.000	0.985	0.985	0.984	0.999	0.996	0.996
$\frac{1}{2}$	1.000	1.000	0.972	1.000	0.994	0.995	0.986	1.000	0.992	0.999
$\frac{1}{4}$	1.000	1.000	0.992	1.000	0.999	0.999	0.995	1.000	0.998	1.000
$\frac{1}{8}$	1.000	1.000	0.998	1.000	1.000	1.000	0.999	1.000	1.000	1.000
$\frac{1}{16}$	1.000	1.000	0.999	1.000	1.000	1.000	1.000	1.000	1.000	1.000

Table 3a. ER with p-order equilibration and $(p+1)$-degree bubble-space: Laplace's equation Range of the effectivity index as a function of the aspect-ratio for the Regular pattern.

ER with p-order equilibration and $(p+1)$-degree bubble-space										
Chevron Pattern										
Aspect Ratio	$p=2$		$p=3$		$p=4$		$p=5$		$p=6$	
	C_L	C_U	C_L	C_U	C_L	C_U	C_L	C_U	C_L	C_U
$\frac{1}{1}$	1.000	1.008	0.948	1.000	0.986	1.109	0.984	0.998	0.995	1.027
$\frac{1}{2}$	1.000	1.009	0.972	1.000	0.994	1.208	0.986	1.000	0.992	1.269
$\frac{1}{4}$	1.000	1.004	0.992	1.000	0.999	1.093	0.995	1.000	0.998	1.241
$\frac{1}{8}$	1.000	1.001	0.998	1.000	1.000	1.025	0.999	1.000	1.000	1.071
$\frac{1}{16}$	1.000	1.000	1.000	1.000	1.000	1.006	1.000	1.000	1.000	1.017

Table 3b. ER with p-order equilibration and $(p+1)$-degree bubble-space: Laplace's equation. Range of the effectivity index as a function of the aspect-ratio for the Chevron pattern.

ER with p-order equilibration and $(p+1)$-degree bubble-space										
Union-Jack Pattern										
Aspect Ratio	$p=2$		$p=3$		$p=4$		$p=5$		$p=6$	
	C_L	C_U	C_L	C_U	C_L	C_U	C_L	C_U	C_L	C_U
$\frac{1}{1}$	1.000	1.000	0.948	1.319	0.986	0.986	0.984	0.999	0.995	0.995
$\frac{1}{2}$	1.000	1.000	0.972	1.179	0.994	0.995	0.986	1.385	0.992	0.999
$\frac{1}{4}$	1.000	1.000	0.992	1.048	0.999	0.999	0.995	1.196	0.998	1.000
$\frac{1}{8}$	1.000	1.000	0.998	1.011	1.000	1.000	0.999	1.049	1.000	1.000
$\frac{1}{16}$	1.000	1.000	1.000	1.003	1.000	1.000	1.000	1.011	1.000	1.000

Table 3c. ER with p-order equilibration and $(p+1)$-degree bubble-space: Laplace's equation. Range of the effectivity index as a function of the aspect-ratio for the Union-Jack pattern.

ER with p-order equilibration and $(p+1)$-degree bubble-space										
Criss-Cross Pattern										
Aspect Ratio	$p=2$		$p=3$		$p=4$		$p=5$		$p=6$	
	C_L	C_U	C_L	C_U	C_L	C_U	C_L	C_U	C_L	C_U
$\frac{1}{1}$	1.000	1.000	0.948	1.319	0.986	0.986	0.984	0.999	0.995	0.995
$\frac{1}{2}$	0.922	0.977	0.902	1.132	0.937	0.941	0.916	1.157	0.961	0.964
$\frac{1}{4}$	0.796	0.985	0.801	0.903	0.825	0.843	0.757	1.000	0.835	0.897
$\frac{1}{8}$	0.733	0.995	0.741	0.822	0.748	0.811	0.667	0.878	0.711	0.855
$\frac{1}{16}$	0.714	0.999	0.717	0.806	0.719	0.805	0.682	0.842	0.694	0.841

Table 3d. ER with p-order equilibration and $(p+1)$-degree bubble-space: Laplace's equation. Range of the effectivity index as a function of the aspect-ratio for the Criss-Cross pattern.

ER with $(p-1)$-order equilibration and $(p+1)$-degree bubble-space										
Chevron Pattern										
Aspect Ratio	$p=2$		$p=3$		$p=4$		$p=5$		$p=6$	
	C_L	C_U	C_L	C_U	C_L	C_U	C_L	C_U	C_L	C_U
$\frac{1}{1}$	1.000	1.008	0.948	1.000	0.986	1.109	0.984	0.998	0.995	1.027
$\frac{1}{2}$	1.000	1.009	0.972	1.000	0.994	1.208	0.986	1.000	0.992	1.269
$\frac{1}{4}$	1.000	1.004	0.992	1.000	0.999	1.093	0.995	1.000	0.998	1.241
$\frac{1}{8}$	1.000	1.001	0.998	1.000	1.000	1.025	0.999	1.000	1.000	1.071
$\frac{1}{16}$	1.000	1.000	1.000	1.000	1.000	1.006	1.000	1.000	1.000	1.017

Table 4a. ER with $(p-1)$-order equilibration and $(p+1)$-degree bubble-space: Laplace's equation. Range of the effectivity index as a function of the aspect-ratio for the Chevron pattern.

ER with $(p-1)$-order equilibration and $(p+1)$-degree bubble-space										
Union-Jack Pattern										
Aspect Ratio	$p=2$		$p=3$		$p=4$		$p=5$		$p=6$	
	C_L	C_U	C_L	C_U	C_L	C_U	C_L	C_U	C_L	C_U
$\frac{1}{1}$	1.000	1.000	0.948	1.319	0.986	0.986	0.984	0.999	0.995	0.995
$\frac{1}{2}$	1.000	1.000	0.972	1.179	0.994	0.995	0.986	1.385	0.992	0.999
$\frac{1}{4}$	1.000	1.000	0.992	1.048	0.999	0.999	0.995	1.196	0.998	1.000
$\frac{1}{8}$	1.000	1.000	0.998	1.011	1.000	1.000	0.999	1.049	1.000	1.000
$\frac{1}{16}$	1.000	1.000	1.000	1.003	1.000	1.000	1.000	1.011	1.000	1.000

Table 4b. ER with $(p-1)$-order equilibration and $(p+1)$-degree bubble-space: Laplace's equation. Range of the effectivity index as a function of the aspect-ratio for the Union-Jack pattern.

ER with $(p-1)$-order equilibration and $(p+1)$-degree bubble-space										
Criss-Cross Pattern										
Aspect Ratio	$p=2$		$p=3$		$p=4$		$p=5$		$p=6$	
	C_L	C_U	C_L	C_U	C_L	C_U	C_L	C_U	C_L	C_U
$\frac{1}{1}$	1.000	1.000	0.948	1.319	0.986	0.986	0.984	0.999	0.995	0.995
$\frac{1}{2}$	0.922	0.977	0.902	1.132	0.937	0.941	0.916	1.157	0.961	0.964
$\frac{1}{4}$	0.796	0.985	0.801	0.903	0.825	0.843	0.757	1.000	0.835	0.897
$\frac{1}{8}$	0.733	0.995	0.741	0.822	0.748	0.811	0.667	0.878	0.711	0.855
$\frac{1}{16}$	0.714	0.999	0.717	0.806	0.719	0.805	0.682	0.842	0.694	0.841

Table 4c. ER with $(p-1)$-order equilibration and $(p+1)$-degree bubble-space: Laplace's equation. Range of the effectivity index as a function of the aspect-ratio for the Criss-Cross pattern.

ER with $(p-2)$-order equilibration and $(p+1)$-degree bubble-space								
Union-Jack Pattern								
Aspect Ratio	$p=3$		$p=4$		$p=5$		$p=6$	
	C_L	C_U	C_L	C_U	C_L	C_U	C_L	C_U
$\frac{1}{1}$	0.948	1.033	0.995	0.995	0.984	1.007	0.997	0.997
$\frac{1}{2}$	0.972	1.160	0.994	1.112	0.986	1.080	0.992	1.059
$\frac{1}{4}$	0.992	1.568	0.999	1.414	0.995	1.316	0.998	1.259
$\frac{1}{8}$	0.998	2.551	1.000	2.116	0.999	1.854	1.000	1.692
$\frac{1}{16}$	1.000	4.746	1.000	3.755	1.000	3.143	1.000	2.737

Table 5a. ER with $(p-2)$-order equilibration and $(p+1)$-degree bubble-space: Laplace's equation. Range of the effectivity index as a function of the aspect-ratio for the Union-Jack pattern.

ER with $(p-2)$-order equilibration and $(p+1)$-degree bubble-space								
Criss-Cross Pattern								
Aspect Ratio	$p=3$		$p=4$		$p=5$		$p=6$	
	C_L	C_U	C_L	C_U	C_L	C_U	C_L	C_U
$\frac{1}{1}$	0.948	1.033	0.995	0.995	0.984	1.007	0.997	0.997
$\frac{1}{2}$	0.894	0.930	0.897	0.944	0.899	0.950	0.938	0.958
$\frac{1}{4}$	0.702	0.841	0.692	0.848	0.707	0.869	0.757	0.894
$\frac{1}{8}$	0.512	0.816	0.469	0.812	0.549	0.829	0.536	0.855
$\frac{1}{16}$	0.406	0.810	0.323	0.803	0.493	0.818	0.377	0.841

Table 5b. ER with $(p-2)$-order equilibration and $(p+1)$-degree bubble-space: Laplace's equation. Range of the effectivity index as a function of the aspect-ratio for the Criss-Cross pattern.

ER with p-order equilibration and $(p+1)$-degree polynomial space										
Regular Pattern										
Aspect Ratio	$p=2$		$p=3$		$p=4$		$p=5$		$p=6$	
	C_L	C_U	C_L	C_U	C_L	C_U	C_L	C_U	C_L	C_U
$\frac{1}{1}$	1.281	1.541	1.000	1.412	1.047	1.269	1.047	1.155	1.012	1.123
$\frac{1}{2}$	1.339	1.487	1.089	1.408	1.045	1.373	1.003	1.325	1.005	1.269
$\frac{1}{4}$	1.339	1.508	1.265	1.398	1.192	1.392	1.124	1.385	1.086	1.378
$\frac{1}{8}$	1.306	1.558	1.319	1.463	1.325	1.398	1.282	1.379	1.236	1.382
$\frac{1}{16}$	1.295	1.575	1.323	1.509	1.342	1.461	1.351	1.419	1.350	1.389

Table 6a. ER with p-order equilibration and $(p+1)$-degree polynomial space: Laplace's equation. Range of the effectivity index as a function of the aspect-ratio for the Regular pattern.

ER with p-order equilibration and $(p+1)$-degree polynomial space										
Chevron Pattern										
Aspect Ratio	$p=2$		$p=3$		$p=4$		$p=5$		$p=6$	
	C_L	C_U	C_L	C_U	C_L	C_U	C_L	C_U	C_L	C_U
$\frac{1}{1}$	1.409	1.417	1.000	1.412	1.163	1.246	1.047	1.155	1.069	1.092
$\frac{1}{2}$	1.407	1.419	1.179	1.334	1.091	1.417	1.008	1.321	1.011	1.419
$\frac{1}{4}$	1.342	1.508	1.299	1.365	1.291	1.342	1.243	1.279	1.196	1.402
$\frac{1}{8}$	1.306	1.559	1.321	1.462	1.338	1.405	1.337	1.325	1.333	1.334
$\frac{1}{16}$	1.295	1.575	1.323	1.509	1.342	1.468	1.352	1.418	1.360	1.396

Table 6b. ER with p-order equilibration and $(p+1)$-degree polynomial space: Laplace's equation. Range of the effectivity index as a function of the aspect-ratio for the Chevron pattern.

ER with p-order equilibration and $(p+1)$-degree polynomial space										
Union-Jack Pattern										
Aspect Ratio	$p=2$		$p=3$		$p=4$		$p=5$		$p=6$	
	C_L	C_U	C_L	C_U	C_L	C_U	C_L	C_U	C_L	C_U
$\frac{1}{1}$	1.417	1.417	1.000	1.547	1.163	1.163	1.047	1.155	1.069	1.069
$\frac{1}{2}$	1.407	1.423	1.179	1.405	1.091	1.337	1.008	1.545	1.011	1.264
$\frac{1}{4}$	1.342	1.507	1.299	1.391	1.291	1.301	1.243	1.382	1.196	1.284
$\frac{1}{8}$	1.306	1.558	1.321	1.472	1.338	1.385	1.337	1.359	1.287	1.334
$\frac{1}{16}$	1.295	1.575	1.323	1.512	1.342	1.461	1.352	1.429	1.359	1.379

Table 6c. ER with p-order equilibration and $(p+1)$-degree polynomial space: Laplace's equation. Range of the effectivity index as a function of the aspect-ratio for the Union-Jack pattern.

ER with p-order equilibration and $(p+1)$-degree polynomial space										
Criss-Cross Pattern										
Aspect Ratio	$p=2$		$p=3$		$p=4$		$p=5$		$p=6$	
	C_L	C_U	C_L	C_U	C_L	C_U	C_L	C_U	C_L	C_U
$\frac{1}{1}$	1.417	1.417	1.000	1.547	1.163	1.163	1.047	1.155	1.069	1.069
$\frac{1}{2}$	1.271	1.724	1.401	1.451	1.256	1.338	1.169	1.369	1.175	1.182
$\frac{1}{4}$	1.235	1.958	1.242	1.881	1.166	1.839	1.253	1.556	1.138	1.569
$\frac{1}{8}$	1.227	2.047	1.186	2.158	1.129	2.200	1.160	1.977	1.099	2.014
$\frac{1}{16}$	1.225	2.073	1.173	2.265	1.121	2.352	1.133	2.299	1.085	2.342

Table 6d. ER with p-order equilibration and $(p+1)$-degree polynomial space: Laplace's equation. Range of the effectivity index as a function of the aspect-ratio for the Criss-Cross pattern.

ER with $(p-1)$-order equilibration and $(p+1)$-degree polynomial space				
Quartic elements				
Aspect Ratio	Union-Jack		Criss-Cross	
	C_L	C_U	C_L	C_U
$\frac{1}{1}$	1.126	1.126	1.126	1.126
$\frac{1}{2}$	1.121	1.223	1.256	1.759
$\frac{1}{4}$	1.165	1.399	1.566	3.496
$\frac{1}{8}$	1.241	1.483	1.785	7.132
$\frac{1}{16}$	1.308	1.497	1.868	14.376

Table 7. ER with $(p-1)$-order equilibration and $(p+1)$-degree polynomial space: Laplace's equation. Range of the effectivity index as a function of the aspect-ratio for the Union-Jack and the Criss-Cross pattern.

ER with linear equilibration and $(p+1)$-degree bubble-space								
Cubic elements								
Grid-material orientation θ	Regular Pattern		Chevron Pattern		Union-Jack Pattern		Criss-Cross Pattern	
	C_L	C_U	C_L	C_U	C_L	C_U	C_L	C_U
0	.948	1.000	.948	9.194	.948	9.194	.368	1.033
5	.945	1.000	.948	3.136	.948	2.863	.457	1.033
10	.935	1.000	.949	1.607	.948	1.234	.609	1.033
15	.920	1.000	.948	1.059	.855	1.052	.701	1.033
20	.903	1.000	.702	1.032	.780	1.034	.736	1.033
25	.891	1.000	.619	1.024	.736	1.033	.780	1.034
30	.886	1.000	.564	1.020	.701	1.033	.855	1.052
35	.883	1.000	.526	1.018	.609	1.033	.948	1.234
40	.881	1.000	.561	1.017	.457	1.033	.948	2.863
45	.881	1.000	.641	1.017	.368	1.033	.948	9.194
50	.881	1.000	.725	1.017	.457	1.033	.948	2.863
55	.883	1.000	.526	1.018	.609	1.033	.948	1.234
60	.886	1.000	.567	1.020	.701	1.033	.855	1.052
65	.882	1.000	.619	1.024	.736	1.033	.780	1.034
70	.891	1.000	.702	1.032	.780	1.034	.736	1.033
75	.908	1.000	.948	1.059	.855	1.052	.701	1.033
80	.935	1.000	.948	1.607	.948	1.234	.609	1.033
85	.945	1.000	.948	3.136	.948	2.863	.457	1.033
90	.948	1.000	.948	9.194	.948	9.194	.368	1.033

Table 8a. ER with linear equilibration and $(p+1)$-degree bubble-space: Orthotropic heat-conduction ($1. \leq K_{min} \leq K_{max} \leq 1000.$), "harmonic" solutions, cubic elements. Range of the effectivity-index for the four patterns as a function of the grid-material orientation.

ER with p-order equilibration and $(p+1)$-degree bubble-space								
Cubic elements								
Grid-material orientation θ	Regular Pattern		Chevron Pattern		Union-Jack Pattern		Criss-Cross Pattern	
	C_L	C_U	C_L	C_U	C_L	C_U	C_L	C_U
0	.948	1.000	.948	1.000	.948	1.319	.710	1.319
5	.945	1.000	.948	1.000	.948	1.319	.723	1.319
10	.935	1.000	.836	1.000	.879	1.319	.716	1.319
15	.920	1.000	.707	1.000	.814	1.319	.711	1.319
20	.903	1.000	.642	1.000	.764	1.319	.729	1.319
25	.891	1.000	.592	1.000	.729	1.319	.764	1.319
30	.886	1.000	.547	1.000	.711	1.319	.814	1.319
35	.883	1.000	.517	1.000	.716	1.319	.879	1.319
40	.881	1.000	.562	1.000	.723	1.319	.955	1.319
45	.881	1.000	.627	1.000	.710	1.319	.948	1.319
50	.881	1.000	.724	1.000	.723	1.319	.955	1.319
55	.883	1.000	.807	1.000	.716	1.319	.879	1.319
60	.886	1.000	.547	1.000	.711	1.319	.814	1.319
65	.882	1.000	.592	1.000	.729	1.319	.764	1.319
70	.891	1.000	.642	1.000	.764	1.319	.729	1.319
75	.908	1.000	.707	1.000	.814	1.319	.711	1.319
80	.935	1.000	.836	1.000	.879	1.319	.716	1.319
85	.945	1.000	.948	1.000	.955	1.319	.723	1.319
90	.948	1.000	.948	1.000	.948	1.319	.710	1.319

Table 8b. ER with p-order equilibration and $(p+1)$-degree bubble-space: Orthotropic heat-conduction ($1. \leq K_{min} \leq K_{max} \leq 1000.$), "harmonic" solutions, cubic elements. Range of the effectivity-index for the four patterns as a function of the grid-material orientation.

ER with linear equilibration and $(p+1)$-degree polynomial space								
Cubic elements								
Grid-material orientation θ	Regular Pattern		Chevron Pattern		Union-Jack Pattern		Criss-Cross Pattern	
	C_L	C_U	C_L	C_U	C_L	C_U	C_L	C_U
0	1.000	1.527	1.000	22.087	1.000	22.140	1.000	34.699
5	1.000	5.361	1.000	21.025	1.000	19.379	1.000	33.102
10	1.000	10.894	1.000	18.335	1.000	12.595	1.000	28.936
15	1.000	14.925	1.000	15.324	1.000	11.675	1.000	23.462
20	1.000	17.750	1.000	16.763	1.000	14.684	1.000	18.337
25	1.000	19.568	1.000	19.546	1.000	18.337	1.000	14.684
30	1.000	20.775	1.000	21.827	1.000	23.462	1.000	11.675
35	1.000	21.631	1.000	24.216	1.000	28.936	1.000	12.595
40	1.000	22.180	1.000	27.936	1.000	33.102	1.000	19.379
45	1.000	22.373	1.000	30.648	1.000	34.699	1.000	22.140
50	1.000	22.180	1.000	27.935	1.000	33.102	1.000	19.379
55	1.000	21.631	1.000	24.216	1.000	28.936	1.000	12.595
60	1.000	20.775	1.000	21.827	1.000	23.462	1.000	11.675
65	1.000	19.568	1.000	19.545	1.000	18.337	1.000	14.684
70	1.000	17.750	1.000	16.762	1.000	14.684	1.000	18.337
75	1.000	14.925	1.000	15.319	1.000	11.675	1.000	23.462
80	1.000	10.894	1.000	18.335	1.000	12.595	1.000	28.936
85	1.000	5.896	1.000	21.025	1.000	19.379	1.000	33.102
90	1.000	1.528	1.000	22.087	1.000	22.140	1.000	34.699

Table 8c. ER with linear equilibration and $(p+1)$-degree polynomial space: Orthotropic heat-conduction ($1. \leq K_{min} \leq K_{max} \leq 1000.$), "harmonic" solutions, cubic elements. Range of the effectivity-index for the four patterns as a function of the grid-material orientation.

ER with p-order equilibration and $(p+1)$-degree polynomial space								
Cubic elements								
Grid-material orientation θ	Regular Pattern		Chevron Pattern		Union-Jack Pattern		Criss-Cross Pattern	
	C_L	C_U	C_L	C_U	C_L	C_U	C_L	C_U
0	1.000	1.522	1.000	1.523	1.000	1.547	1.000	2.295
5	1.000	5.832	1.000	5.640	1.000	5.369	1.000	6.617
10	1.000	10.578	1.000	10.260	1.000	8.311	1.000	10.268
15	1.000	14.338	1.000	14.114	1.000	9.263	1.000	11.515
20	1.000	17.104	1.000	17.037	1.000	10.026	1.000	11.141
25	1.000	19.028	1.000	18.904	1.000	11.141	1.000	10.026
30	1.000	20.278	1.000	19.650	1.000	11.515	1.000	9.263
35	1.000	21.017	1.000	19.264	1.000	10.268	1.000	8.311
40	1.000	21.390	1.000	17.974	1.000	6.617	1.000	5.369
45	1.000	21.502	1.000	16.649	1.000	2.295	1.000	1.547
50	1.000	21.390	1.000	17.974	1.000	6.617	1.000	5.369
55	1.000	21.017	1.000	19.264	1.000	10.268	1.000	8.311
60	1.000	20.278	1.000	19.650	1.000	11.515	1.000	9.263
65	1.000	19.028	1.000	18.904	1.000	11.141	1.000	10.026
70	1.000	17.104	1.000	17.037	1.000	10.026	1.000	11.141
75	1.000	14.338	1.000	14.114	1.000	9.263	1.000	11.515
80	1.000	10.578	1.000	10.260	1.000	8.311	1.000	10.268
85	1.000	5.832	1.000	5.663	1.000	5.369	1.000	6.617
90	1.000	1.523	1.000	1.412	1.000	1.547	1.000	2.295

Table 8d. ER with p-order equilibration and $(p+1)$-degree polynomial space: Orthotropic heat-conduction ($1. \leq K_{min} \leq K_{max} \leq 1000.$), "harmonic" solutions, cubic elements. Range of the effectivity-index for the four patterns as a function of the grid-material orientation.

ER with p-order equilibration and $(p+2)$-degree polynomial-space				
Cubic elements				
Grid-material orientation θ	Estimator based on the optimal constant		Estimator based on Ladeveze's recipe	
	Regular Pattern	Criss-Cross Pattern	Regular Pattern	Criss-Cross Pattern
	C_U	C_U	C_U	C_U
0	1.522 (1.424)	2.296	1.489 (1.514)	2.296
5	5.295	6.606	5.851	6.694
10	8.487	10.370	10.821	10.390
15	14.354	11.535	15.149	11.583
20	17.130	11.661	18.607	11.793
25	19.065	11.701	21.183	11.991
30	20.326	10.361	22.725	10.865
35	21.075	8.313	23.259	8.731
40	21.454	5.315	22.803	5.393
45	21.568	1.523	21.567	1.701
50	21.454	5.315	22.803	5.393
55	21.075	8.313	23.260	8.731
60	20.326	10.361	22.725	10.865
65	19.065	11.700	21.183	11.989
70	17.130	11.661	18.641	11.793
75	14.354	11.535	15.149	11.583
80	10.585	10.370	10.822	10.390
85	5.833	6.606	5.851	6.694
90	1.517 (1.424)	2.296	1.489 (1.514)	2.296

Table 9. ER with p-order equilibration and $(p+2)$-degree polynomial equilibration and p-order polynomial-space: Orthotropic heat-conduction ($1. \leq K_{min} \leq K_{max} \leq 1000.$), "harmonic" solutions, cubic elements. Range of the effectivity-index for the Regular and the Criss-Cross pattern as a function of the grid-material orientation. The terms in the parentheses were computed using $(p+3)$-polynomial space.

ER with 0-order equilibration and (p+3)-degree polynomial space		
Criss-Cross pattern		
Cubic elements		
Aspect Ratio	C_L	C_U
$\frac{1}{1}$	1.000	4.583
$\frac{1}{2}$	1.338	2.773
$\frac{1}{4}$	1.685	4.636
$\frac{1}{8}$	1.931	8.744
$\frac{1}{16}$	2.030	17.207

Table 10. ER with 0-order equilibration and $(p + 3)$-degree polynomial space: Laplaces equation, Criss-Cross pattern, cubic elements. Range of the effectivity index as a function of the aspect-ration for the Criss-Cross pattern.

ER with linear equilibration and (p+1)-degree bubble-space						
Regular Pattern						
Aspect Ratio	$p = 2$		$p = 3$		$p = 4$	
	C_L	C_U	C_L	C_U	C_L	C_U
$\frac{1}{1}$	1.000	1.000	1.000	1.000	1.000	1.000
$\frac{1}{2}$	1.000	1.000	1.000	1.000	1.000	1.000
$\frac{1}{4}$	1.000	1.000	1.000	1.000	1.000	1.000
$\frac{1}{8}$	1.000	1.000	1.000	1.000	1.000	1.000
$\frac{1}{16}$	1.000	1.000	1.000	1.000	1.000	1.000

Table 11a. ER with linear equilibration and $(p + 1)$-degree bubble-space: Elasticity problem, "harmonic" solution. Range of the effectivity index as a function of the aspect-ratio for the Regular pattern.

ER with linear equilibration and $(p+1)$-degree bubble-space						
Chevron Pattern						
Aspect Ratio	$p=2$		$p=3$		$p=4$	
	C_L	C_U	C_L	C_U	C_L	C_U
$\frac{1}{1}$	0.915	1.011	0.997	1.201	0.989	1.249
$\frac{1}{2}$	0.905	1.032	0.982	1.882	0.993	1.658
$\frac{1}{4}$	0.951	1.018	1.000	3.668	1.000	2.333
$\frac{1}{8}$	0.985	1.006	1.000	7.667	1.000	4.820
$\frac{1}{16}$	0.996	1.002	1.000	15.649	1.000	10.602

Table 11b. ER with linear equilibration and $(p+1)$-degree bubble-space: Elasticity problem, "harmonic" solution. Range of the effectivity index as a function of the aspect-ratio for the Chevron pattern.

ER with linear equilibration and $(p+1)$-degree bubble-space						
Union-Jack Pattern						
Aspect Ratio	$p=2$		$p=3$		$p=4$	
	C_L	C_U	C_L	C_U	C_L	C_U
$\frac{1}{1}$	0.929	0.992	1.019	1.451	0.980	1.063
$\frac{1}{2}$	0.948	0.997	0.998	1.879	0.997	1.441
$\frac{1}{4}$	0.978	0.999	0.999	3.239	1.000	2.514
$\frac{1}{8}$	0.994	1.000	1.000	7.148	1.000	5.280
$\frac{1}{16}$	0.998	1.000	1.000	15.308	1.000	10.991

Table 11c. ER with linear equilibration and $(p+1)$-degree bubble-space: Elasticity problem, "harmonic" solutions. Range of the effectivity index as a function of the aspect-ratio for the Union-Jack pattern.

ER with linear equilibration and $(p+1)$-degree bubble-space						
Criss-Cross Pattern						
Aspect Ratio	$p=2$		$p=3$		$p=4$	
	C_L	C_U	C_L	C_U	C_L	C_U
$\frac{1}{1}$	0.945	0.992	1.034	1.451	0.985	1.063
$\frac{1}{2}$	0.806	0.999	0.884	1.352	0.925	1.011
$\frac{1}{4}$	0.737	0.996	0.739	1.013	0.811	0.994
$\frac{1}{8}$	0.715	0.999	0.674	0.854	0.720	0.914
$\frac{1}{16}$	0.709	1.000	0.653	0.819	0.687	0.859

Table 11d. ER with linear equilibration and $(p+1)$-degree bubble-space: Elasticity problem, "harmonic" solutions. Range of the effectivity index as a function of the aspect-ratio for the Criss-Cross pattern.

ER with p-order equilibration and (p+1)-degree bubble-space						
Regular Pattern						
Aspect Ratio	$p=2$		$p=3$		$p=4$	
	C_L	C_U	C_L	C_U	C_L	C_U
$\frac{1}{1}$	1.000	1.000	1.000	1.000	1.000	1.000
$\frac{1}{2}$	1.000	1.000	1.000	1.000	1.000	1.000
$\frac{1}{4}$	1.000	1.000	1.000	1.000	1.000	1.000
$\frac{1}{8}$	1.000	1.000	1.000	1.000	1.000	1.000
$\frac{1}{16}$	1.000	1.000	1.000	1.000	1.000	1.000

Table 12a. ER with p-order equilibration and $(p+1)$-degree bubble-space: Elasticity problem, "harmonic" solution. Range of the effectivity index as a function of the aspect-ratio for the Regular pattern.

ER with p-order equilibration $(p+1)$-degree bubble-space						
Chevron Pattern						
Aspect Ratio	$p=2$		$p=3$		$p=4$	
	C_L	C_U	C_L	C_U	C_L	C_U
$\frac{1}{1}$	0.915	1.011	0.999	1.066	0.990	1.129
$\frac{1}{2}$	0.905	1.032	0.886	1.031	0.946	1.253
$\frac{1}{4}$	0.951	1.018	0.919	1.002	0.925	1.188
$\frac{1}{8}$	0.985	1.006	0.970	1.000	0.955	1.053
$\frac{1}{16}$	0.996	1.002	0.992	1.000	0.984	1.013

Table 12b. ER with p-order equilibration and $(p+1)$-degree bubble-space: Elasticity problem, "harmonic" solution. Range of the effectivity index as a function of the aspect-ratio for the Chevron pattern.

ER with p-order equilibration and (p+1)-degree bubble-space						
Union-Jack Pattern						
Aspect Ratio	$p=2$		$p=3$		$p=4$	
	C_L	C_U	C_L	C_U	C_L	C_U
$\frac{1}{1}$	0.929	0.992	0.984	1.268	0.945	1.077
$\frac{1}{2}$	0.948	0.997	0.901	1.299	0.910	1.047
$\frac{1}{4}$	0.978	0.999	0.928	1.127	0.914	1.004
$\frac{1}{8}$	0.994	1.000	0.969	1.029	0.957	1.000
$\frac{1}{16}$	0.998	1.000	0.990	1.007	0.986	1.000

Table 12c. ER with p-order equilibration and $(p+1)$-degree bubble-space: Elasticity problem, "harmonic" solutions. Range of the effectivity index as a function of the aspect-ratio for the Union-Jack pattern.

ER with p-order equilibration and $(p+1)$-degree bubble-space						
Criss-Cross Pattern						
Aspect Ratio	$p=2$		$p=3$		$p=4$	
	C_L	C_U	C_L	C_U	C_L	C_U
$\frac{1}{1}$	0.945	0.992	0.984	1.268	0.945	1.079
$\frac{1}{2}$	0.806	0.999	0.880	1.272	0.846	1.180
$\frac{1}{4}$	0.737	0.996	0.811	1.076	0.808	1.115
$\frac{1}{8}$	0.715	0.999	0.743	0.952	0.818	1.144
$\frac{1}{16}$	0.709	1.000	0.717	0.817	0.749	0.984

Table 12d. ER with p-order equilibration and $(p+1)$-degree bubble-space: Elasticity problem, "harmonic" solutions. Range of the effectivity index as a function of the aspect-ratio for the Criss-Cross pattern.

ER with linear equilibration and $(p+3)$-degree polynomial space								
Cubic element								
Aspect Ratio	Regular Pattern		Chevron Pattern		Union-Jack Pattern		Criss-Cross Pattern	
	C_L	C_U	C_L	C_U	C_L	C_U	C_L	C_U
$\frac{1}{1}$	1.061	2.803	1.231	3.661	1.411	4.373	1.423	4.373
$\frac{1}{2}$	1.089	4.217	1.529	8.211	1.274	8.383	1.339	10.059
$\frac{1}{4}$	1.022	8.201	2.129	28.229	2.291	24.943	1.206	39.633
$\frac{1}{8}$	1.005	16.171	2.909	115.549	2.875	107.956	1.155	166.903
$\frac{1}{16}$	1.001	32.162	3.034	471.452	3.039	461.886	1.156	681.244

Table 13a. ER with linear equilibration and $(p+3)$-degree polynomial space: Elasticity problem, "harmonic" solutions, cubic elements. Range of the effectivity index for the four patterns as a function of the aspect-ratio.

ER with p-order equilibration and full (p+3) space								
Cubic element								
Aspect Ratio	Regular Pattern		Chevron Pattern		Union-Jack Pattern		Criss-Cross Pattern	
	C_L	C_U	C_L	C_U	C_L	C_U	C_L	C_U
$\frac{1}{1}$	1.361	2.590	1.623	2.254	1.508	2.088	1.508	2.088
$\frac{1}{2}$	1.177	3.695	1.351	2.419	1.283	3.362	1.375	4.168
$\frac{1}{4}$	1.023	7.034	1.246	6.165	1.123	7.039	1.564	9.703
$\frac{1}{8}$	1.003	13.616	1.124	13.074	1.035	13.654	2.577	20.748
$\frac{1}{16}$	1.001	26.921	1.041	26.622	1.007	26.945	2.946	42.385

Table 13b. ER with p-order equilibration and $(p+3)$-degree polynomial space: Elasticity problem, "harmonic" solutions, cubic elements. Range of the effectivity index for the four patterns as a function of the aspect-ratio.

ER with p-order equilibration using the optimal constants and $(p+3)$-degree polynomial space								
Cubic element								
Aspect Ratio	Regular Pattern		Chevron Pattern		Union-Jack Pattern		Criss-Cross Pattern	
	C_L	C_U	C_L	C_U	C_L	C_U	C_L	C_U
$\frac{1}{1}$	1.358	2.251	1.486	2.253	1.389	1.558	1.398	1.576
$\frac{1}{2}$	1.134	2.544	1.336	1.991	1.263	1.733	1.356	3.024
$\frac{1}{4}$	1.019	4.112	1.245	3.641	1.100	3.062	1.212	6.597
$\frac{1}{8}$	1.002	7.294	1.124	7.017	1.025	5.538	1.274	13.215
$\frac{1}{16}$	1.001	13.651	1.041	13.504	1.006	9.901	1.306	25.568

Table 14. ER with p-order equilibration uusing the optimal constants and $(p+3)$-degree polynomial-space: Elasticity problem, "harmonic" solutions, cubic elements. Range of the effectivity index for the four patterns as function of the aspect-ratio.

Mesh-cell at mesh interface						
Cubic elements of the Tensor-product family						
Grid-material orientation θ	$ER-B$		$ER1B$		$ER3B$	
	C_L	C_U	C_L	C_U	C_L	C_U
-90.0	1.00808	1.05823	1.00806	1.03806	1.00806	1.00806
-80.0	1.03738	1.09775	1.03742	1.08768	1.03743	1.03768
-70.0	1.03288	1.17191	1.01595	1.14957	1.01614	1.14744
-60.0	1.02945	1.41395	1.02932	1.39318	1.01734	1.19251
-50.0	1.04011	2.07578	1.04596	2.03430	1.02194	1.23450
-40.0	1.04983	2.28256	1.05117	2.20244	1.01196	1.30230
-30.0	1.06226	1.80877	1.06454	1.80878	1.00804	1.20877
-20.0	1.08601	1.54419	1.08606	1.47620	1.00710	1.17612
-10.0	1.15133	1.42458	1.15147	1.35448	1.00097	1.11417
0.0	1.19723	1.37793	1.21104	1.31723	1.00836	1.06134
10.0	1.15135	1.42163	1.15135	1.35173	1.00080	1.11417
20.0	1.08594	1.54437	1.08593	1.47639	1.00710	1.17612
30.0	1.06237	1.80872	1.06261	1.80872	1.00653	1.20890
40.0	1.05074	2.28297	1.05233	2.20165	1.01228	1.30170
50.0	1.04019	2.07578	1.04367	2.03429	1.02198	1.23450
60.0	1.03276	1.41442	1.03195	1.39379	1.01719	1.18998
70.0	1.03241	1.16788	1.01624	1.14720	1.01020	1.14679
80.0	1.03747	1.09750	1.03750	1.08777	1.03751	1.03778
90.0	1.00808	1.05848	1.00806	1.03806	1.00806	1.00806

Table 15a. The estimators ER−B, ER1B, ERpB for meshes of square-elements with local refinements: Sensitivity to the material-orthotropy for the three element types. Poisson's equation, mesh-cell at the mesh-interface shown in Fig. 6a, cubic elements ($p = 3$)of the tensor-product family. Range of the effectivity index as a function of the grid-material orientation for $\frac{K_{max}}{K_{min}} = 100$.

Mesh-cell at mesh interface						
Cubic elements of the Serendipity family						
Grid-material orientation θ	$ER-B$		$ER1B$		$ER3B$	
	C_L	C_U	C_L	C_U	C_L	C_U
-90.0	.45030	1.81325	.65034	1.01030	1.00299	1.00299
-80.0	.57480	1.93323	.77476	1.03129	1.00000	1.02013
-70.0	.63578	2.37235	.93547	1.17736	1.00002	1.08318
-60.0	.84709	2.79243	1.04713	1.49640	1.00075	1.12035
-50.0	.95734	3.15292	1.05772	1.75192	1.00990	1.17681
-40.0	1.08648	4.21326	1.08641	2.44247	1.07883	1.23234
-30.0	.99596	3.68377	1.09593	1.88771	1.06093	1.18993
-20.0	.82493	3.30364	1.12495	1.50364	1.04825	1.13941
-10.0	.75818	2.99357	1.15817	1.29552	1.03379	1.09494
0.0	.61412	2.37870	1.16011	1.16010	1.01940	1.07940
10.0	.75819	2.99359	1.15884	1.29552	1.03383	1.09547
20.0	.82490	3.30366	1.12836	1.50356	1.04824	1.13976
30.0	.99596	3.68374	1.09554	1.88784	1.06069	1.18003
40.0	1.08642	4.21328	1.08606	2.44232	1.07817	1.23169
50.0	.95734	3.15297	1.05583	1.75235	1.01004	1.17724
60.0	.84708	2.79237	1.04716	1.49614	1.00209	1.12100
70.0	.63576	2.37229	.93583	1.17737	1.00014	1.08280
80.0	.57482	1.93340	.77521	1.03128	1.00025	1.02012
90.0	.45031	1.81333	.65032	1.01031	1.00299	1.00299

Table 15b. The estimators ER−B, ER1B, ERpB for meshes of square-elements with local refinements: Sensitivity to the material-orthotropy for the three element types. Poisson's equation, mesh-cell at the mesh-interface shown in Fig. 6a, cubic elements ($p = 3$)of the serendipity family. Range of the effectivity index as a function of the grid-material orientation for $\frac{K_{max}}{K_{min}} = 100$.

Mesh-cell at mesh interface						
Cubic elements of the Intermediate family						
Grid-material orientation θ	$ER-B$		$ER1B$		$ER3B$	
	C_L	C_U	C_L	C_U	C_L	C_U
-90.0	1.00646	1.19619	1.00619	1.13627	1.00804	1.09803
-80.0	1.02773	1.22792	1.02773	1.18722	1.03747	1.11723
-70.0	1.03000	1.32004	1.02117	1.24701	1.01612	1.16716
-60.0	1.02358	1.42660	1.00758	1.31664	1.01735	1.21258
-50.0	1.03656	1.73228	1.01656	1.60241	1.02194	1.25450
-40.0	1.05695	2.50016	1.02641	2.26031	1.01190	1.33234
-30.0	1.07807	1.98485	1.04833	1.83414	1.00809	1.30871
-20.0	1.09611	1.86558	1.07451	1.66352	1.00711	1.25612
-10.0	1.13179	1.70922	1.11121	1.52940	1.00096	1.21419
0.0	1.27109	1.57109	1.18316	1.42842	1.00835	1.18134
10.0	1.13197	1.70673	1.11121	1.52346	1.00082	1.21415
20.0	1.09617	1.86507	1.07544	1.66489	1.00713	1.25611
30.0	1.07941	1.98440	1.04836	1.83343	1.00653	1.30897
40.0	1.05705	2.49968	1.02727	2.25884	1.01224	1.33172
50.0	1.03744	1.73254	1.01697	1.60207	1.02193	1.25453
60.0	1.02205	1.42647	1.00199	1.31722	1.01717	1.21999
70.0	1.01294	1.31744	1.01334	1.24693	1.01023	1.16672
80.0	1.02779	1.22801	1.02829	1.18717	1.03755	1.11770
90.0	1.00624	1.19631	1.00672	1.13344	1.00807	1.09806

Table 15c. The estimators ER−B, ER1B, ERpB for meshes of square-elements with local refinements: Sensitivity to the material-orthotropy for the three element types. Poisson's equation, mesh-cell at the mesh-interface shown in Fig. 6a, cubic elements ($p = 3$) of the intermediate family. Range of the effectivity index as a function of the grid-material orientation for $\frac{K_{max}}{K_{min}} = 100$.

Mesh-cell at mesh interface						
Quartic elements of the Tensor-product family						
Grid-material orientation θ	$ER-B$		$ER1B$		$ER4B$	
	C_L	C_U	C_L	C_U	C_L	C_U
-90.0	1.01512	1.01520	1.00505	1.01561	1.00194	1.00891
-80.0	1.01811	1.07782	1.00856	1.04707	1.00743	1.03572
-70.0	1.02510	1.23828	1.00536	1.17824	1.01021	1.09113
-60.0	1.03977	1.70711	1.00977	1.40742	1.01727	1.11901
-50.0	1.05275	2.71473	1.00214	1.81469	1.02195	1.14497
-40.0	1.06121	2.93948	1.00105	2.23961	1.03193	1.22426
-30.0	1.06493	2.37050	1.00433	2.07077	1.01281	1.15825
-20.0	1.07503	1.85533	1.00522	1.79591	1.00793	1.13654
-10.0	1.10495	1.54454	1.00476	1.47406	1.00095	1.11423
0.0	1.22068	1.48029	1.00056	1.31031	1.00882	1.09182
10.0	1.10770	1.54488	1.00747	1.47463	1.00086	1.11418
20.0	1.07510	1.85575	1.00584	1.79518	1.00717	1.13611
30.0	1.06494	2.36943	1.00422	2.07032	1.01253	1.15893
40.0	1.06008	2.93890	1.00051	2.23889	1.03195	1.22394
50.0	1.05225	2.71435	1.00283	1.81441	1.02194	1.14456
60.0	1.03954	1.70695	1.00994	1.40694	1.01789	1.11897
70.0	1.02531	1.23811	1.00506	1.17816	1.01020	1.09678
80.0	1.01567	1.07786	1.00521	1.04788	1.00753	1.03562
90.0	1.01512	1.01692	1.00503	1.01634	1.00194	1.00893

Table 16a. The estimators ER−B, ER1B, ERpB for meshes of square-elements with local refinements: Sensitivity to the material-orthotropy for the three element types. Poisson's equation, mesh-cell at the mesh-interface shown in Fig. 6a, quartic elements ($p = 4$) of the tensor-product family. Range of the effectivity index as a function of the grid-material orientation for $\frac{K_{max}}{K_{min}} = 100$.

Mesh-cell at mesh interface						
Quartic elements of the Serendipity family						
Grid-material orientation θ	$ER-B$		$ER1B$		$ER4B$	
	C_L	C_U	C_L	C_U	C_L	C_U
-90.0	.41231	1.82975	.52232	1.92924	1.00087	1.00094
-80.0	.50482	1.93265	.61485	2.13246	1.00192	1.00973
-70.0	.54283	2.40713	.74286	2.64717	1.00946	1.02536
-60.0	.61126	2.91525	.81123	2.91521	1.01560	1.16481
-50.0	.67252	3.39188	.91251	3.39122	1.03621	1.19702
-40.0	.73732	4.47956	.94730	4.14954	1.04669	1.24909
-30.0	.66297	3.96152	.86293	3.76155	1.03985	1.17035
-20.0	.60244	3.41097	.83246	3.31040	1.03274	1.14661
-10.0	.61420	2.92150	.81427	2.72127	1.03081	1.12464
0.0	.54512	2.63115	.80510	2.41464	1.02692	1.11610
10.0	.61420	2.92150	.81429	2.72153	1.03081	1.12701
20.0	.60244	3.41097	.83243	3.31091	1.03824	1.14505
30.0	.66297	3.96152	.86291	3.76159	1.04053	1.16866
40.0	.73732	4.47956	.94734	4.14920	1.04631	1.24937
50.0	.67252	3.39188	.91253	3.39183	1.03662	1.19744
60.0	.61126	2.91525	.81129	2.91521	1.01532	1.16461
70.0	.54283	2.40713	.74280	2.64415	1.00893	1.02687
80.0	.50482	1.93265	.61489	2.13266	1.00183	1.00952
90.0	.41231	1.82975	.52233	1.92429	1.00084	1.00094

Table 16b. The estimators ER−B, ER1B, ERpB for meshes of square-elements with local refinements: Sensitivity to the material-orthotropy for the three element types. Poisson's equation, mesh-cell at the mesh-interface shown in Fig. 6a, quartic elements ($p = 4$) of the serendipity family. Range of the effectivity index as a function of the grid-material orientation for $\frac{K_{max}}{K_{min}} = 100$.

Mesh-cell at mesh interface						
Quartic elements of the Intermediate family						
Grid-material orientation θ	$ER-B$		$ER1B$		$ER4B$	
	C_L	C_U	C_L	C_U	C_L	C_U
-90.0	1.0170	1.1956	1.0154	1.1456	1.0019	1.0089
-80.0	1.0145	1.4270	1.0148	1.2170	1.0074	1.0357
-70.0	1.0293	1.6582	1.0315	1.4582	1.0102	1.0911
-60.0	1.0377	2.2074	1.0429	1.9074	1.0172	1.1490
-50.0	1.0571	3.1146	1.0516	2.4146	1.0219	1.1949
-40.0	1.0660	3.4396	1.0680	3.0396	1.0319	1.2842
-30.0	1.0633	2.9647	1.0573	2.6647	1.0128	1.2082
-20.0	1.0752	2.2559	1.0667	2.0559	1.0079	1.1365
-10.0	1.1097	1.9440	1.1097	1.6440	1.0009	1.1142
0.0	1.2275	1.6803	1.1075	1.4803	1.0088	1.0918
10.0	1.1014	1.9446	1.1106	1.6446	1.0008	1.1141
20.0	1.0758	2.2551	1.0658	2.0551	1.0071	1.1361
30.0	1.0602	2.9693	1.0572	2.6693	1.0125	1.2089
40.0	1.0665	3.4388	1.0679	3.0388	1.0319	1.2839
50.0	1.0508	3.1144	1.0516	2.4144	1.0219	1.1945
60.0	1.0379	2.2069	1.0429	1.9069	1.0178	1.1489
70.0	1.0260	1.6581	1.0314	1.4581	1.0102	1.0967
80.0	1.0142	1.4278	1.0148	1.2178	1.0075	1.0356
90.0	1.0170	1.1960	1.0154	1.1460	1.0019	1.0089

Table 16c. The estimators ER−B, ER1B, ERpB for meshes of square-elements with local refinements: Sensitivity to the material-orthotropy for the three element types. Poisson's equation, mesh-cell at the mesh-interface shown in Fig. 6a, quartic elements ($p = 4$) of the intermediate family. Range of the effectivity index as a function of the grid-material orientation for $\frac{K_{max}}{K_{min}} = 100$.

Mesh-cell at mesh interface						
Quintic elements of the Tensor-product family						
Grid-material orientation θ	$ER-B$		$ER1B$		$ER5B$	
	C_L	C_U	C_L	C_U	C_L	C_U
-90.0	1.0050	1.1056	1.0043	1.0966	1.0014	1.0094
-80.0	1.0185	1.3770	1.0144	1.1271	1.0064	1.0427
-70.0	1.0253	1.6682	1.0251	1.2642	1.0126	1.0891
-60.0	1.0397	1.9074	1.0393	1.4044	1.0172	1.1190
-50.0	1.0521	2.7446	1.0525	2.1418	1.0246	1.1449
-40.0	1.0610	3.4386	1.0996	3.0319	1.0289	1.2242
-30.0	1.0943	2.9707	1.0945	2.4417	1.0128	1.1582
-20.0	1.1752	2.1559	1.0758	2.1051	1.0079	1.1365
-10.0	1.2649	1.9440	1.0645	1.8844	1.0009	1.1142
0.0	1.3006	1.6163	1.0903	1.5351	1.0088	1.0987
10.0	1.2677	1.9446	1.0672	1.8844	1.0009	1.1142
20.0	1.1751	2.1551	1.0753	2.1051	1.0078	1.1364
30.0	1.0949	2.9693	1.0940	2.4413	1.0128	1.1583
40.0	1.0600	3.4388	1.0995	3.0319	1.0289	1.2240
50.0	1.0522	2.7444	1.0523	2.1419	1.0246	1.1445
60.0	1.0395	1.9069	1.0398	1.4061	1.0172	1.1189
70.0	1.0253	1.6681	1.0253	1.2641	1.0126	1.0888
80.0	1.0156	1.3778	1.0151	1.1272	1.0065	1.0426
90.0	1.0051	1.1063	1.0043	1.0969	1.0014	1.0094

Table 17a. The estimators ER−B, ER1B, ERpB for meshes of square-elements with local refinements: Sensitivity to the material-orthotropy for the three element types. Poisson's equation, mesh-cell at the mesh-interface shown in Fig. 6a, quintic elements ($p = 5$) of the tensor-product family. Range of the effectivity index as a function of the grid-material orientation for $\frac{K_{max}}{K_{min}} = 10$

Mesh-cell at mesh interface						
Quintic elements in the Serendipity family						
Grid-material orientation θ	$ER-B$		$ER1B$		$ER5B$	
	C_L	C_U	C_L	C_U	C_L	C_U
-90.0	.4012	4.9156	1.0210	1.4116	1.0001	1.0001
-80.0	.4052	5.3132	1.0007	1.4136	1.0011	1.0018
-70.0	.5026	5.8283	1.0066	1.6283	1.0093	1.0255
-60.0	.5256	6.2858	1.0256	1.9848	1.0256	1.1845
-50.0	.6663	7.4978	1.0663	2.3978	1.0666	1.2276
-40.0	.7261	8.2192	1.1261	3.2192	1.0265	1.3196
-30.0	.6893	7.7718	1.1893	2.7718	1.0892	1.2713
-20.0	.6325	6.3169	1.2373	2.3169	1.0388	1.1966
-10.0	.5620	5.8680	1.2620	1.8680	1.0601	1.1662
0.0	.5669	4.9586	1.2669	1.7586	1.0664	1.1337
10.0	.5602	5.8659	1.2602	1.8689	1.0599	1.1672
20.0	.6371	6.3171	1.2371	2.3171	1.0387	1.1959
30.0	.6900	7.7684	1.1900	2.7684	1.0909	1.2686
40.0	.7262	8.2195	1.1263	3.2194	1.0262	1.3196
50.0	.6682	7.4975	1.0681	2.3975	1.0668	1.2275
60.0	.5261	6.2847	1.0261	1.9847	1.0258	1.1845
70.0	.4065	5.8285	1.0065	1.6283	1.0063	1.0263
80.0	.4057	5.3135	1.0210	1.4135	1.0008	1.0019
90.0	.4012	4.9116	1.0010	1.4115	1.0001	1.0001

Table 17b. The estimators ER−B, ER1B, ERpB for meshes of square-elements with local refinements: Sensitivity to the material-orthotropy for the three element types. Poisson's equation, mesh-cell at the mesh-interface shown in Fig. 6a, quintic elements ($p = 5$) of the serendipity family. Range of the effectivity index as a function of the grid-material orientation for $\frac{K_{max}}{K_{min}} = 100$.

Mesh-cell with two levels of refinement						
Cubic elements of the Tensor-product family						
Grid-material orientation θ	$ER-B$		$ER1B$		$ER3B$	
	C_L	C_U	C_L	C_U	C_L	C_U
-90.0	1.0250	1.1456	1.0151	1.0461	1.0099	1.0191
-80.0	1.0455	1.3270	1.0173	1.2270	1.0179	1.0412
-70.0	1.0853	1.6682	1.0252	1.4612	1.0202	1.1011
-60.0	1.1397	1.9274	1.0393	1.8277	1.0272	1.2190
-50.0	1.1521	2.7446	1.0525	2.6742	1.0319	1.3449
-40.0	1.1610	3.4386	1.0616	3.0384	1.0519	1.4242
-30.0	1.0943	2.9307	1.0441	2.7307	1.0328	1.3589
-20.0	1.0752	2.1456	1.0357	2.1241	1.0279	1.2365
-10.0	1.0649	1.9441	1.0261	1.7433	1.0109	1.1742
0.0	1.0406	1.7310	1.0200	1.5710	1.0091	1.1018
10.0	1.0677	1.9446	1.0274	1.8352	1.0112	1.1636
20.0	1.0751	2.2456	1.0352	2.1754	1.0282	1.3361
30.0	1.0949	2.9993	1.0444	2.9293	1.0333	1.4568
40.0	1.1600	3.5388	1.0614	3.2391	1.0529	1.5242
50.0	1.1527	2.9444	1.0528	2.8720	1.0341	1.4445
60.0	1.1415	2.1304	1.0394	1.8277	1.0288	1.3183
70.0	1.0877	1.8681	1.0252	1.6616	1.0213	1.2067
80.0	1.0464	1.3978	1.0171	1.4251	1.0184	1.1416
90.0	1.0251	1.1449	1.0151	1.0463	1.0099	1.0191

Table 18a. The estimators ER−B, ER1B, ERpB for meshes of square-elements with local refinements: Sensitivity to the material orthotropy for the three element types. Poisson's equation, periodic mesh-cell with two-levels of refinement shown in Fig. 6b, cubic elements ($p = 3$) of the tensor-product family. Range of the effectivity index as a function of the grid-material orientation for $\frac{K_{max}}{K_{min}} = 100$.

Mesh-cell with two levels of refinement						
Cubic elements of the Serendipity family						
Grid-material orientation θ	$ER-B$		$ER1B$		$ER3B$	
	C_L	C_U	C_L	C_U	C_L	C_U
-90.0	.4016	5.9158	.7226	4.7418	1.0001	1.0002
-80.0	.4251	6.3137	.8051	5.0137	1.0012	1.0018
-70.0	.4824	6.8285	.8524	5.5285	1.0093	1.0172
-60.0	.5052	7.2857	.9262	6.1051	1.0256	1.0856
-50.0	.5662	7.9975	.9366	6.6975	1.0666	1.1094
-40.0	.6461	8.2198	.9461	7.0198	1.0265	1.3001
-30.0	.6292	7.7713	.9292	6.7113	1.0892	1.2183
-20.0	.6125	7.3165	.9135	6.4235	1.0382	1.1604
-10.0	.5922	6.8685	.8922	5.9985	1.0601	1.1586
0.0	.5565	6.5589	.8565	5.4019	1.0664	1.1402
10.0	.5902	6.8655	.9902	5.9955	1.0592	1.1562
20.0	.6125	7.3172	.9135	6.4232	1.0387	1.1959
30.0	.6295	7.7683	.9295	6.7183	1.0909	1.1686
40.0	.6462	8.2195	.9462	7.1101	1.0262	1.2196
50.0	.5689	7.9972	.9359	6.6642	1.0668	1.1072
60.0	.5062	7.6104	.9062	6.0219	1.0252	1.0845
70.0	.4865	6.9421	.8525	5.4120	1.0063	1.0163
80.0	.4252	6.2217	.8052	4.8809	1.0008	1.0019
90.0	.4017	5.9157	.7226	4.7417	1.0001	1.0002

Table 18b. The estimators ER−B, ER1B, ERpB for meshes of square-elements with local refinements: Sensitivity to the material orthotropy for the three element types. Poisson's equation, periodic mesh-cell with two-levels of refinement shown in Fig. 6b, cubic elements ($p = 3$) of the Serendipity family. Range of the effectivity index as a function of the grid-material orientation for $\frac{K_{max}}{K_{min}} = 100$.

Analysis of the effect of the order of equilibration on the value of the effectivity index		
Criss-Cross Pattern; Quartic elements		
Aspect ratio $= \frac{1}{4}$		
Estimator	$\frac{\sum_{i=1}^{4} \|\|\|\hat{e}_{\tau_i} - e_h\|\|\|_{\tau_i}^2}{\sum_{i=1}^{4} \|\|\|e_h\|\|\|_{\tau_i}^2}$	$\frac{2\sum_{i=1}^{4} b_{\tau_i}(\hat{e}_{\tau_i} - e_h, e_h)}{\sum_{i=1}^{4} \|\|\|e_h\|\|\|_{\tau_i}^2}$
Solution $= Q_1 + 0Q_2$		
ER1B	3.155727	-3.437173
ERpB	3.133369	-3.422308
ER1Pp+3	14.044716	-4.000000
ERpPp+3	4.587711	-4.000000
Solution $= 0Q_1 + Q_2$		
ER1B	2.435774	-2.957068
ERpB	2.646988	-2.966098
ER1Pp+3	5.184388	-4.000000
ERpPp+3	7.359869	-4.000000

Table 19. Analysis of the effect of the order of equilibration on the value of the effectivity index: Lapalce's equation, quartic elements, Criss-Cross pattern, aspect ratio $= \frac{1}{4}$. The square of the effectivity index in the pattern is:

$$\kappa^2(c(x^0, h), u_h, f) = 1 + \frac{\sum_{i=1}^{4} \|\|\|\hat{e}_{\tau_i} - e_h\|\|\|_{\tau_i}^2}{\sum_{i=1}^{4} \|\|\|e_h\|\|\|_{\tau_i}^2} + \frac{2\sum_{i=1}^{4} b_{\tau}(\hat{e}_{\tau_i} - e_h, e_h)}{\sum_{i=1}^{4} \|\|\|e_h\|\|\|_{\tau_i}^2}$$

Above we give the values of the second and third term of the above expansion for the harmonic monomial $Q_1(x_1, x_2) = \mathcal{R}e((x_1+ix_2)^5)$ and $Q_2(x_1, x_2) = \mathcal{I}m((x_1+ix_2)^5)$.

Equilibrated patch-residual estimator				
Criss-Cross Pattern; Cubic elements				
Grid orientation θ	Linear equilibration		p-order equilibration	
	C_L	C_U	C_L	C_U
0	1.000	1.596	1.000	1.022
5	.988	3.065	.998	1.471
10	.974	2.188	.999	1.270
15	.967	1.608	.999	1.151
20	.987	1.953	.999	1.105
25	.996	1.395	.999	1.035
30	.997	1.418	1.000	1.156
35	.983	1.436	1.000	1.334
40	.989	1.428	.999	1.427
45	.995	1.077	.991	1.123
50	.988	1.428	.999	1.427
55	.983	1.436	1.000	1.334
60	.997	1.417	1.000	1.156
65	.997	1.395	.999	1.035
70	.987	1.954	.999	1.105
75	.968	1.608	.999	1.151
80	.974	2.188	.997	1.270
85	.988	3.066	.998	1.471
90	1.000	1.596	1.000	1.022

Table 20. The equilibrated patch-residual estimator with elementwise $(p+1)$-polynomial space: Orthtropic heat-conduction ($1. \leq K_{min} \leq K_{max} \leq 1000.$), "harmonic" solutions, cubic elements, Criss-Cross pattern. Comparison of the range of the effectivity index as a function of the grid-material orientation for the estimator based on linear and p-order equilibration.

List of Figures

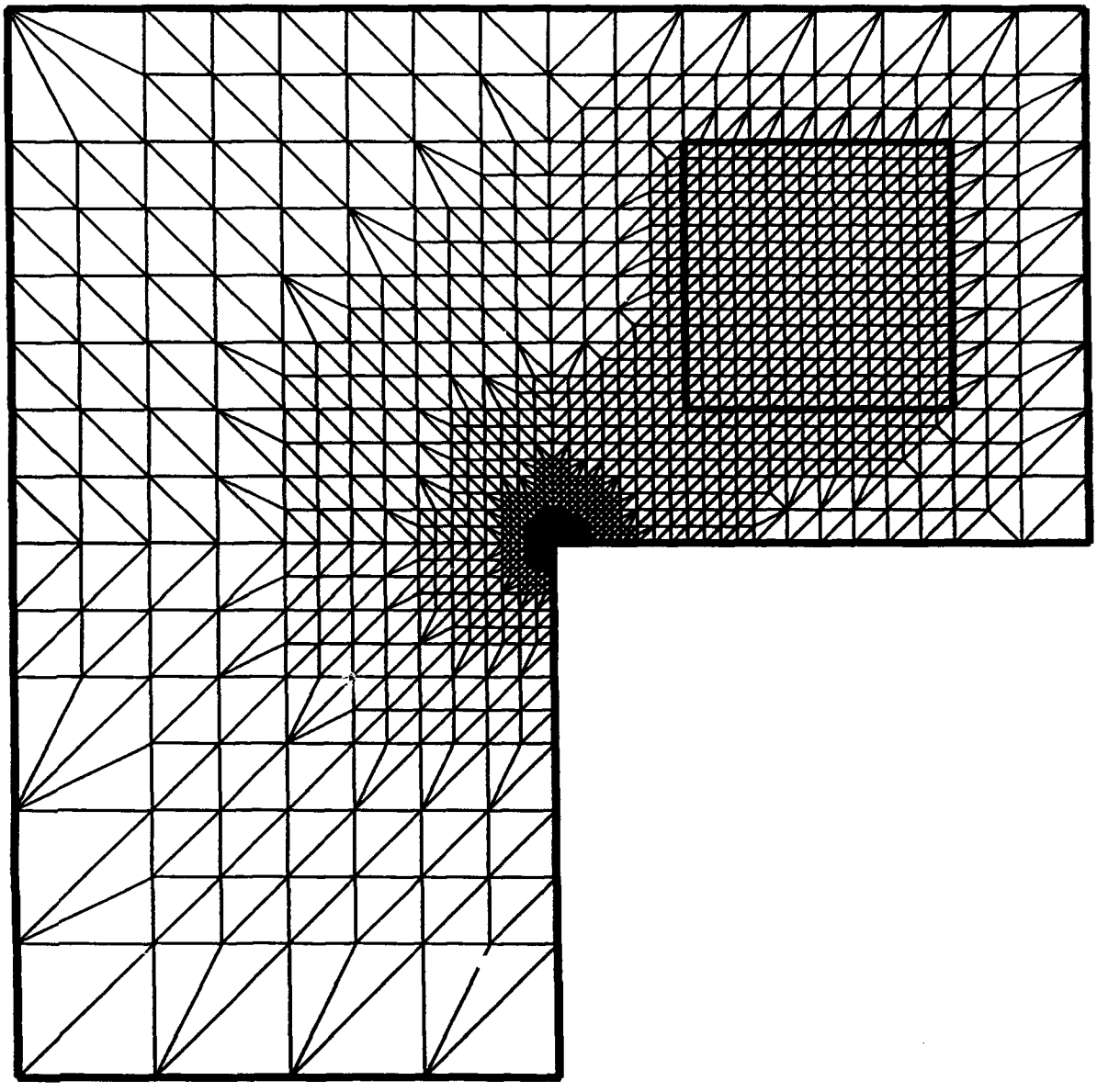

Fig. 1

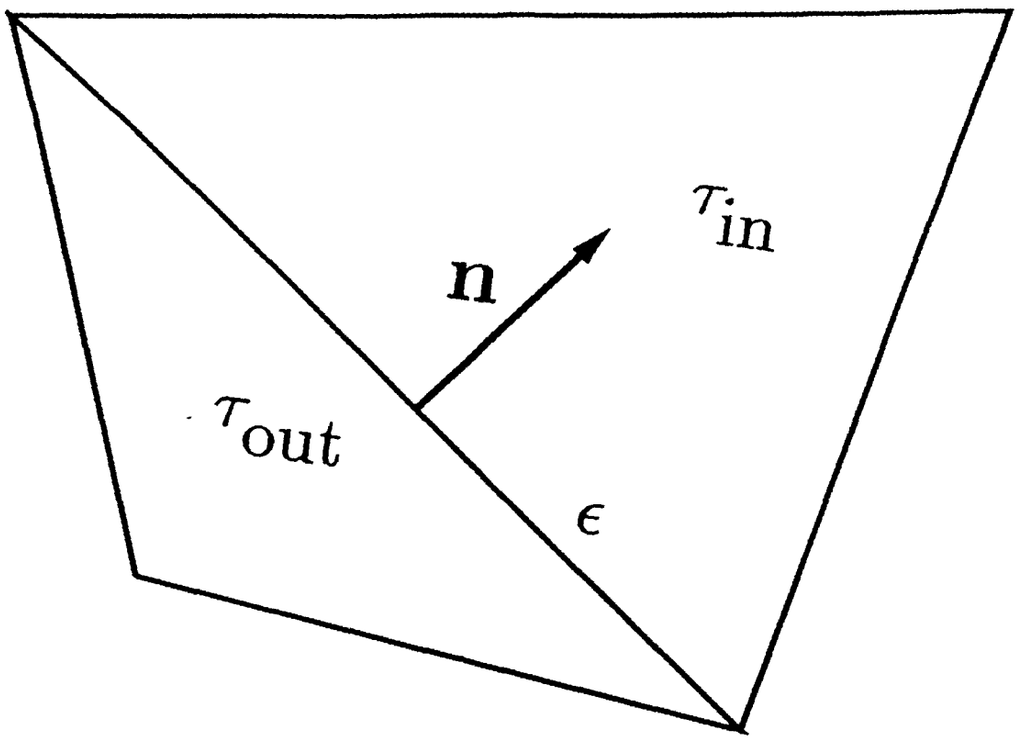

Fig. 2

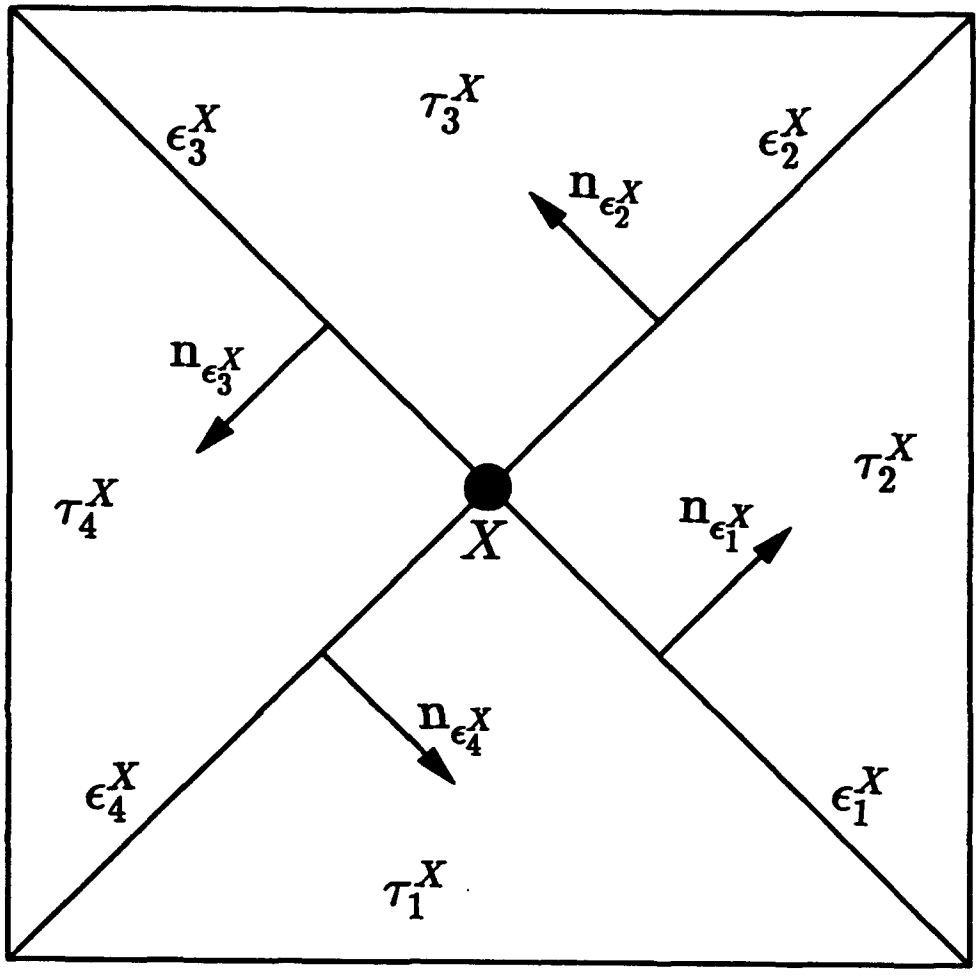
ϵ_3^X
τ_3^X
ϵ_2^X
$\mathbf{n}_{\epsilon_2^X}$
$\mathbf{n}_{\epsilon_3^X}$
τ_4^X
X
τ_2^X
$\mathbf{n}_{\epsilon_1^X}$
$\mathbf{n}_{\epsilon_4^X}$
ϵ_4^X
ϵ_1^X
τ_1^X

Fig. 3

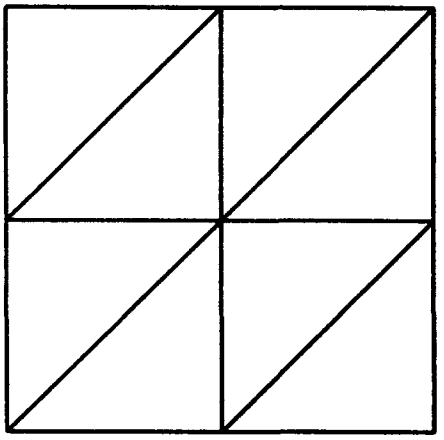

(a)

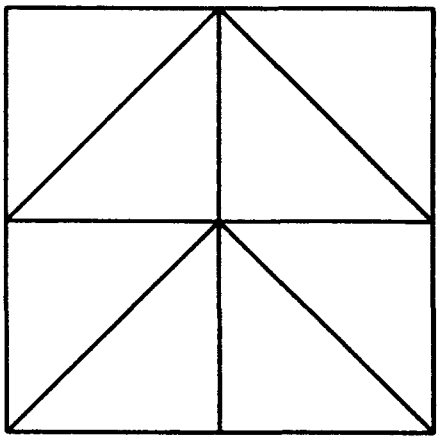

(b)

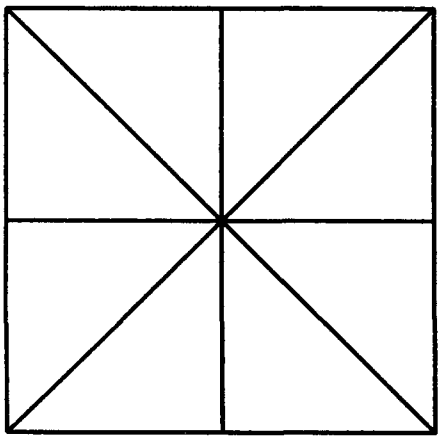

(c)

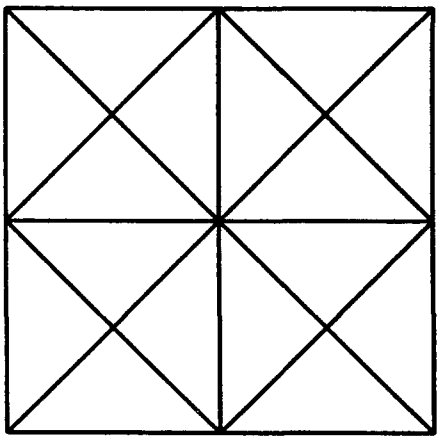

(d)

Fig. 4

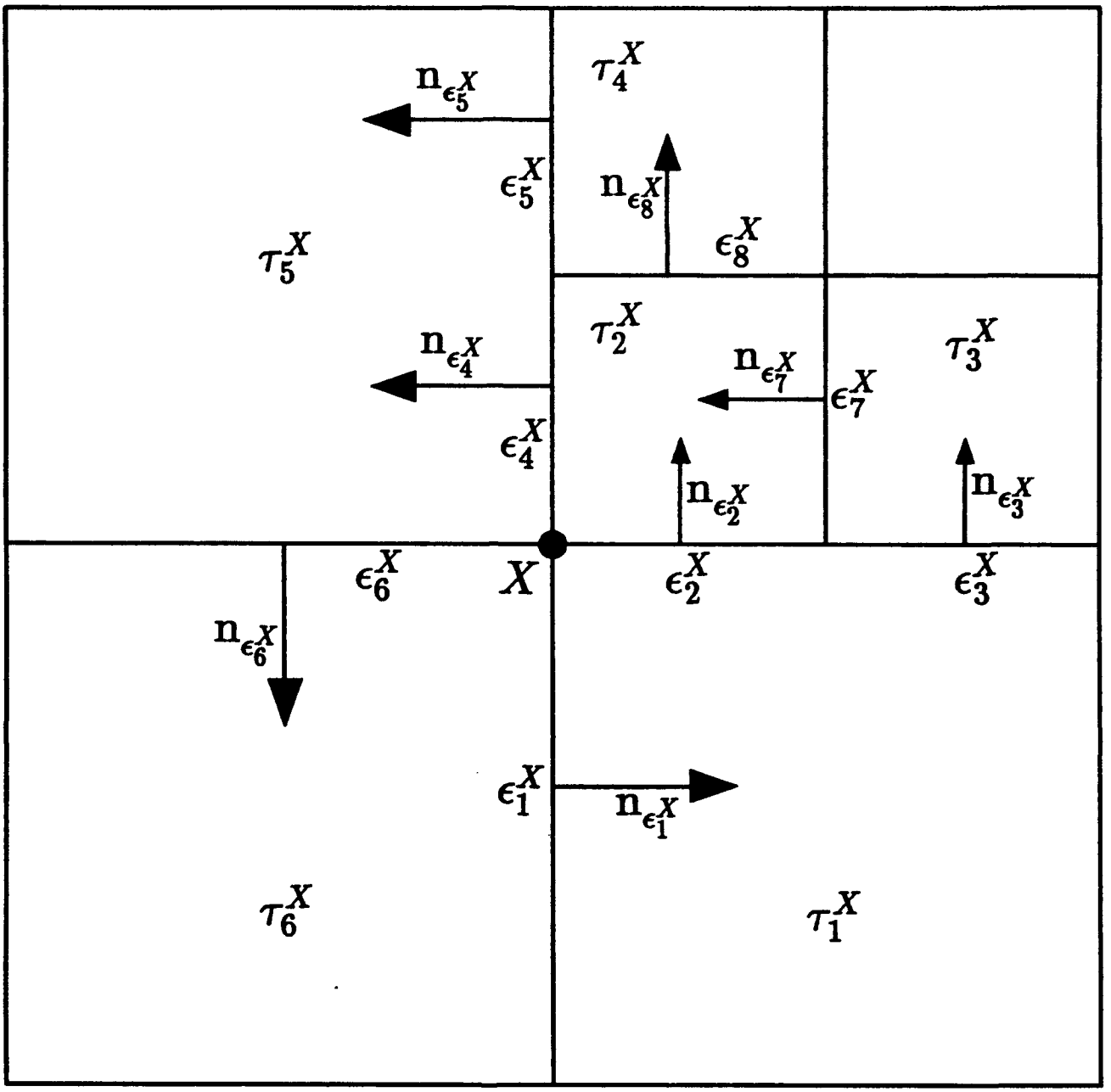
τ_4^X
$n_{\epsilon_5^X}$
ϵ_5^X
$n_{\epsilon_8^X}$
ϵ_8^X
τ_5^X
τ_2^X
τ_3^X
$n_{\epsilon_4^X}$
$n_{\epsilon_7^X}$
ϵ_7^X
ϵ_4^X
$n_{\epsilon_2^X}$
$n_{\epsilon_3^X}$
ϵ_6^X
X
ϵ_2^X
ϵ_3^X
$n_{\epsilon_6^X}$
ϵ_1^X
$n_{\epsilon_1^X}$
τ_6^X
τ_1^X

Fig. 5a

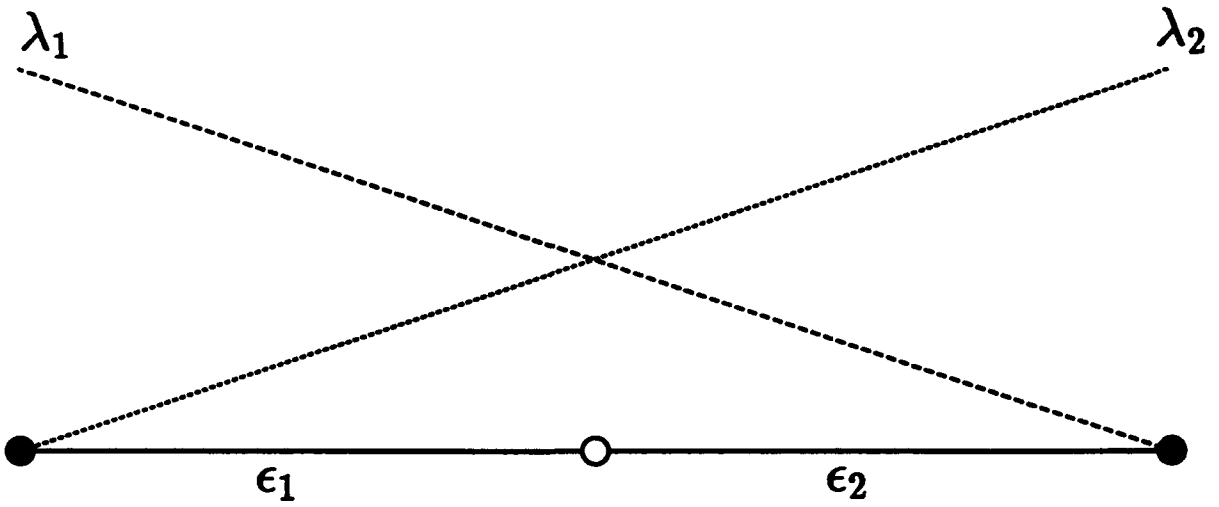

Fig. 5b

Fig. 6a

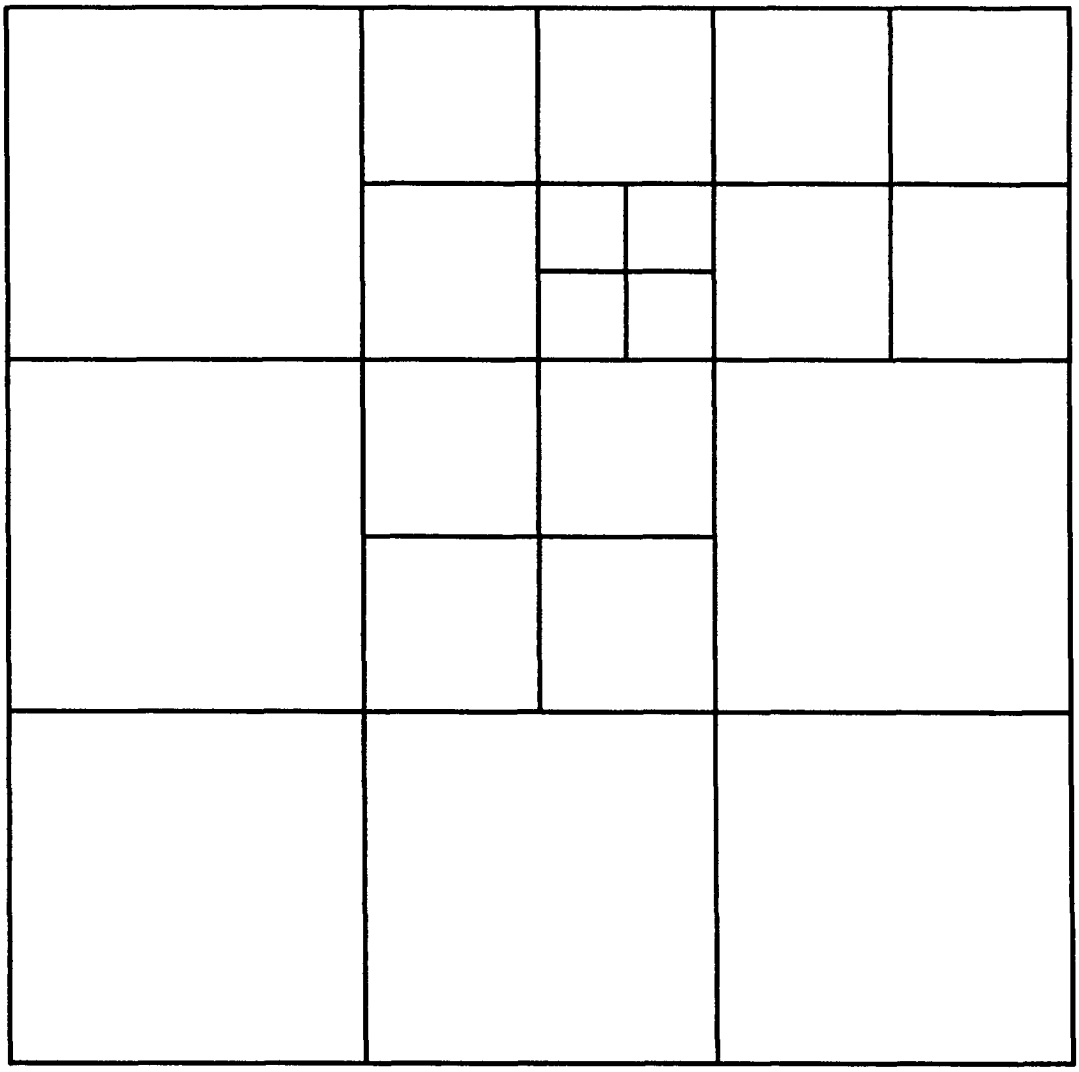

Fig. 6b

The Laboratory for Numerical Analysis is an integral part of the Institute for Physical Science and Technology of the University of Maryland, under the general administration of the Director, Institute for Physical Science and Technology. It has the following goals:

To conduct research in the mathematical theory and computational implementation of numerical analysis and related topics, with emphasis on the numerical treatment of linear and nonlinear differential equations and problems in linear and nonlinear algebra.

To help bridge gaps between computational directions in engineering, physics, etc., and those in the mathematical community.

To provide a limited consulting service in all areas of numerical mathematics to the University as a whole, and also to government agencies and industries in the State of Maryland and the Washington Metropolitan area.

To assist with the education of numerical analysts, especially at the postdoctoral level, in conjunction with the Interdisciplinary Applied Mathematics Program and the programs of the Mathematics and Computer Science Departments. This includes active collaboration with government agencies such as the National Institute of Standards and Technology.

To be an international center of study and research for foreign students in numerical mathematics who are supported by foreign governments or exchange agencies (Fulbright, etc.).

Further information may be obtained from **Professor I. Babuška**, Chairman, Laboratory for Numerical Analysis, Institute for Physical Science and Technology, University of Maryland, College Park, Maryland 20742-2431.